NASA TECHNICAL NOTE

NASA TN D-1968

NASA TN D-1968

IN-FLIGHT SHOCK-WAVE PRESSURE MEASUREMENTS ABOVE AND BELOW A BOMBER AIRPLANE AT MACH NUMBERS FROM 1.42 TO 1.69

by Domenic J. Maglieri, Virgil S. Ritchie, and John F. Bryant, Jr.
Langley Research Center
Langley Station, Hampton, Va.

NATIONAL AERONAUTICS AND SPACE ADMINISTRATION • WASHINGTON, D. C. • OCTOBER 1963

TECHNICAL NOTE D-1968

IN-FLIGHT SHOCK-WAVE PRESSURE MEASUREMENTS ABOVE AND BELOW A BOMBER AIRPLANE AT MACH NUMBERS FROM 1.42 TO 1.69

By Domenic J. Maglieri, Virgil S. Ritchie,
and John F. Bryant, Jr.

Langley Research Center
Langley Station, Hampton, Va.

NATIONAL AERONAUTICS AND SPACE ADMINISTRATION

NATIONAL AERONAUTICS AND SPACE ADMINISTRATION

TECHNICAL NOTE D-1968

IN-FLIGHT SHOCK-WAVE PRESSURE MEASUREMENTS ABOVE AND BELOW A BOMBER AIRPLANE AT MACH NUMBERS FROM 1.42 TO 1.69

By Domenic J. Maglieri, Virgil S. Ritchie,
and John F. Bryant, Jr.

SUMMARY

In-flight shock-wave pressure surveys have been made above and below a bomber airplane at distances of approximately 1,300 to 2,000 feet, and also below the bomber airplane at distances of about 4,600 to 9,100 feet. Measured pressure signatures are presented for the bomber airplane in the Mach number range from 1.42 to 1.69 with a gross-weight range from about 83,000 to 117,000 pounds.

The pressure waves measured below the airplane had higher peak positive values than those measured above the airplane at comparable distances. For data obtained below the airplane the measured positive impulses were generally larger than the negative impulses, whereas the reverse was true above the airplane. The combined lift-volume calculations for the far field are in good agreement with the pressure measurements made above and below the airplane. Such a result would be expected for airplane operating conditions in which lift effects are significant. The results also indicate that as the distance from the airplane increases, the wavelength (distance between bow and tail waves) increases and the number of individual shock waves diminishes until the classical N-wave shape is approximated at a distance of 50 to 90 body lengths for the conditions of these tests.

INTRODUCTION

The sonic boom is a serious operating problem for current supersonic military airplanes and may also be a serious operating problem for future supersonic transport airplanes. The prediction of sonic-boom pressures for proposed configurations involves both the lift and volume components. The manner in which these lift and volume components combine is shown by the theory to be important but has not to date been verified by experiment. Experimental verification by means of available far-field data is difficult, and hence a knowledge of the pertinent details of the pressure field near the airplane is desirable.

A method of computing the sonic-boom pressures, based on the pressure fields about bodies of revolution in a homogeneous atmosphere and taking into account only volume effects, has been developed by Whitham (ref. 1). This work was

extended by Walkden (ref. 2) to include lift effects and radial asymmetry, as for winged bodies. The methods of reference 2 were used in making predictions for specific airplane configurations by Morris (ref. 3) and Crosthwait (ref. 4), and some comparisons with experimental results are also presented in reference 4. Some in-flight pressure measurements at distances from about 100 to 1,800 feet below and to the side of a fighter airplane have been reported by Mullens (ref. 5). In-flight pressure data for a bomber airplane taken at a distance of 200 feet to the side are presented by Smith in reference 6 and compared with the results of near-field calculations. Pressure measurements for fighter-type airplanes at very low altitudes over a ground instrumentation array are presented by Maglieri, Huckel, and Parrott in reference 7. Several wind-tunnel studies have been made for winged bodies at various angles of attack, and the results have been compared with theory by Carlson (refs. 8, 9, and 10) and Ryhming (refs. 11 and 12). However, the in-flight results to date have applied to flight conditions for which the evaluation of the lift and volume effects could not be conveniently accomplished.

The present paper contains some well-documented pressure data for a delta-wing bomber airplane for which precise measurements of position and operating conditions, as well as environmental atmospheric conditions, are available. Special effort was made to obtain data for various lift-coefficient conditions and measuring locations so that lift-volume interactions could be evaluated. Special instrumentation capable of measuring small pressure changes was used, and data were obtained at distances for which atmospheric effects were minimized and for which direct comparison could be made with theory and with future wind-tunnel experiments. Appendix B by Virgil S. Ritchie gives a detailed description of the unique instrumentation probe used to obtain the pressure measurements along with the corresponding static and wind-tunnel calibrations.

SYMBOLS

A	area of bomber-airplane section obtained by oblique cut for a nominal Mach number of 1.65, sq ft
C_L	lift coefficient of generating airplane
h	vertical distance from ground to airplane, ft
Δh	vertical separation distance between generating and probe airplanes (positive when probe airplane is below generating airplane), ft
I	pressure impulse obtained by integrating signature of bomber airplane, lb-sec/sq ft
l	length of bomber airplane, ft
M	airplane Mach number
ΔM	differential Mach number between generating and probe airplanes

p_p ambient pressure at altitude of probe airplane, lb/sq ft

p_g ambient pressure at altitude of generating airplane, lb/sq ft

Δp peak positive overpressure, lb/sq ft

Δs horizontal separation distance between generating and probe airplanes, ft

Δt time interval between bow and tail shock waves of bomber airplane in horizontal plane, sec

V airplane ground velocity, ft/sec

ΔV differential ground velocity between generating and probe airplanes, ft/sec

W gross weight of bomber airplane, lb

X distance between bow and tail shock waves of bomber airplane in horizontal plane (wavelength), ft

x axial distance from nose of airplane, ft

y separation distance between generating airplane and probe airplane, measured perpendicular to generating-airplane flight track (positive when probe airplane is below generating airplane), $\sqrt{(\Delta h)^2 + (\Delta s)^2}$, ft

Subscripts:

1 value indicated by pressure gage 1

2 value indicated by pressure gage 2

pos positive

neg negative

APPARATUS AND METHODS

Generating and Probe Airplanes

A delta-wing bomber having an external store as shown in figure 1 was used as the generating airplane. Sketches of the plan view, front view, and profile view of the airplane are shown in figure 2, and calculated area-distribution curves based on oblique cuts at a Mach number of 1.65 for positions both above and below the airplane are given in figure 3. The airplane has an overall length of 96.8 feet and a total wing area of 1,542 square feet.

The fighter airplane shown in figure 4(a) was used with a specially instrumented nose-boom probe for sensing pressure changes during flights through the flow field of the bomber airplane. The special nose-boom pressure probe is shown in figure 4(b). In-flight recording instrumentation was located in the rocket bay of the airplane.

Both the bomber and the fighter airplane were based at Edwards Air Force Base, Calif., and were operated by personnel of the Air Force Flight Test Center.

Pressure-Measuring Instrumentation

The specially instrumented nose-boom probe was designed, fabricated, and calibrated by NASA personnel. Details of the pressure probe and of wind-tunnel tests to determine the pressure-sensing characteristics of the probe are described in appendixes A and B. The general arrangement and main dimensions of the probe components are illustrated schematically in figure 5. (Symbols used in fig. 5 are defined in appendix B.) Two NASA inductance-type miniature pressure gages were contained in the probe at locations near pressure-sensing orifices. The probe was laboratory checked before installation on the airplane to establish its sensitivity to changes in temperature and ambient pressure and its sensitivity to a vibration environment. The pressure probe was equipped with conical tip 1 (fig. 5) for some of the in-flight measurements (flights 4 to 7) and alternate conical tip 2 for others (flights 1 to 3).

Flight-Test Procedures

The tests were arranged in such a way that the pressure field of the bomber airplane was probed by the measuring airplane within the range of the Askania optical tracking network located at Edwards Air Force Base. (See fig. 6.) The speed and altitude of the generating airplane were kept constant during the measurements. The instrumented airplane passed through the pressure field of the generating airplane at incremental Mach numbers from 0.24 to 0.49 while closing from the rear. The fighter-plane pilot, by means of a visual reference, attempted to probe the pressure field of the generating airplane in a vertical plane containing its flight track. The speed and altitude of the probe airplane were likewise held as steady as possible during the penetration. The pressure-measurement system on the instrumented airplane was kept inert from the time of take-off until steady flight conditions were established. (See appendix A for details.) Just prior to penetration of the pressure field of the generating airplane, the pilot of the probe airplane was instructed by radio to activate the pressure-measurement system. In addition, he transmitted a timing signal to the ground tracking station both prior to and subsequent to penetration. This timing signal was superposed on the tracking data and the data record of the flight recorder.

Flight-test conditions.- The flight tests were conducted during clear weather to allow good optical tracking, and furthermore only incipient turbulence was encountered on all flights above 35,000 feet. At lower altitudes some mild turbulence was encountered by the instrumented airplane.

One of the objectives of the tests was to obtain data for as wide a range as possible of lift coefficients of the generating airplane. This was accomplished during the tests by first flying the generating airplane with maximum fuel load at the highest altitude consistent with airplane performance. After data were obtained for these flight conditions, the airplane was flown in a holding pattern until the excess fuel had been consumed, and then a low-altitude test was conducted at the lighter weight. For these flight conditions pressure-field surveys were made above and below the generating airplane at distances of approximately 1,300 to 2,000 feet, and below the airplane at distances of about 4,600 to 9,100 feet.

Table I describes the ranges of altitude, Mach number, true ground speed, and heading of the two airplanes as well as the gross weights and calculated lift coefficients of the generating airplane and the separation distances between the two airplanes.

Space Positioning

During the flight tests, both radar and optical (Askania) tracking were accomplished. The radar plotting-board tracks were used for ground control of the airplanes while they were getting into the proper position for the test run. These tracks were used further during the actual data recording as a basis for instructions to the pilot of the instrumented airplane to activate the pressure-sensing equipment and the time-synchronization signal. The Askania tracking data were used in the data-reduction process for determining the speeds and positions of the airplanes during the actual recording of data. One Askania network of three stations was used to track the generating airplane, and a second Askania network of three stations was used to track the instrumented airplane. Four frames per second were obtained, and provision was made in the data reduction for applying position corrections within each frame in order to determine the space position with a quoted accuracy of ±1 foot and airplane velocity within an accuracy of ±1 foot per second. By means of machine computing, the relative positions of the two airplanes as a function of time could be obtained from the tracking data for the individual airplanes. Reduction of the tracking data was accomplished by computing personnel of the Air Force Flight Test Center. Sample tracking data showing airplane altitudes, velocities, and lateral positions as a function of time are given in figure 7 for one of the flights. Also indicated are the positions of the two airplanes at the time of initial penetration and at the end of penetration of the pressure field of the generating airplane.

Weather Soundings

Weather data were obtained from rawinsonde soundings accomplished within 3 hours of the time of the flights. From such soundings atmospheric pressure and temperature were measured and the speed of sound and the components of wind velocity parallel to and perpendicular to the flight track were computed. These data are given in table II for the air space between, and 1,000 feet above and below, the generating and probe airplanes for each run. In general the atmospheric conditions were quite stable at the altitude of the tests, and no extreme

weather conditions were encountered. The flight headings were such that headwinds were encountered on each flight.

DISCUSSION OF IN-FLIGHT RESULTS

Measured wave shapes, peak positive overpressures, impulses, and wavelength data are presented. The time histories of the differential pressures are reproduced in figures 8 to 15, and some of the significant quantities such as peak positive overpressure, positive and negative impulses, and wavelength are listed in table III. The measured peak positive overpressures and wavelengths are compared with available theory in figures 16 and 17, respectively, and a correlation of the pressure time histories with airplane geometry is shown in figure 18.

Wave Shapes

Time histories of the measured pressures are reproduced in figures 8 to 14 for the various flight conditions. In each case the top pressure trace was obtained with gage 1, which was connected to the forward orifices on the measuring boom, whereas the bottom trace was obtained with gage 2, which was connected to the rearward orifices. (See fig. 5.) The two pressure traces are not directly comparable in amplitude because of differences in the sensitivities of the gages and in the reflection factors for the probe at the orifice locations, and possibly because of effects of boundary layer and airplane angle of attack. Adjustments have been made, however, for these differences in the amplitude calibrations. (See appendix B for details.)

Because the data were obtained by penetrating the pressure field from the rear, true time on the records of figures 8 to 14 is represented by the right to left direction. Thus, the tail shock wave was penetrated first and the bow shock wave was penetrated last during the data recording. A 0.10-second time interval is indicated in each figure. Because of the fore-and-aft displacement of the two sets of orifices, penetration of the tail shock wave is indicated by gage 1 a short time ahead of the indication by gage 2. In each figure an attempt has been made to construct a zero line which represents the ambient atmospheric pressure for the conditions of the record. A point of interest in comparing the top and bottom records of these figures (see, for example, fig. 8) is that the top record contains some apparent pressure variations after the penetration of the bow wave. These oscillations occur at the frequency of the first natural bending mode of the boom as it emerges from the pressure field of the generating airplane. These oscillations are more apparent on gage 1 because of the greater flexibility of the boom in the region of the forward orifices. Similar spurious pressure indications were noted when turbulence was encountered and were most prevalent at the lower altitudes. (See, for example, gage 1 of fig. 10.)

The usual features of these measured signatures are a bow wave and tail wave, plus in most cases some additional intermediate waves, the relative locations of which are suggested by the sharp breaks in the pressure traces. The general shapes of these waves are similar to those that have been measured to the side of this same type of generating airplane (ref. 6) and at fairly close distances

below fighter airplanes (refs. 5, 6, and 7). The strength, location, and number of the measured shock waves were found to be functions of the flight conditions and the distance and orientation of the measurements. In order to illustrate some of the observed variations in the measured signatures, figure 15 has been prepared.

In comparing the data of flight 1 and flight 3, for which the lift-coefficient values of the generating airplane were different, it can be seen that the pressure signatures measured below the generating airplane (fig. 15(a)) are also different. In particular, a lesser number of shock waves are present and the wavelength is longer for operation at the higher lift coefficient (flight 1). On the other hand, for approximately the same range of lift coefficients the pressure signatures measured above the airplane (negative values of y) are not widely different. (See fig. 15(b).)

It is of interest that below the airplane (fig. 15(a)) the higher pressures are associated with the higher lift coefficient, whereas the reverse is true above the airplane (fig. 15(b)). These results would be expected if the lift pressures add to the volume pressures below the airplane and subtract from the volume pressures above the airplane. Figure 15(c) shows the rather large differences in pressures below and above the airplane at about the same lift coefficient.

For given flight conditions, there were definite indications that the pressure field was not radially symmetrical about the generating airplane. For instance, the data of flight 3, which were taken below the airplane, vary significantly from the data of flight 5, which were taken above the airplane at about the same lift coefficient (see fig. 15(c)). In particular, the number of pressure peaks is greater and the wavelength is longer for the signature obtained below the airplane.

Another finding of the tests, substantiating the results of reference 5, was that as distance from the generating airplane is increased the shock-wave signature develops from the rather complex near-field pattern to a pattern which tends to resemble a classical N-wave at a distance of 50 to 90 body lengths for the conditions of these tests. (See figs. 8, 13, and 14.)

Peak Positive Overpressures

Values of peak positive overpressure have been determined from the records of figures 8 to 14 and are given for both gage locations in table III. These experimental data are plotted in nondimensional form as a function of separation distance in figure 16. Also shown in figure 16 are the ranges of values calculated by considering combined lift-volume effects for weights from 83,000 to 117,000 pounds, a Mach number of 1.65, altitudes of 40,000 to 48,500 feet, and standard atmospheric conditions. These calculations are represented by the hatched area for positive lift coefficients (below aircraft) and the cross-hatched area for negative lift coefficients (above aircraft). The combined lift-volume far-field calculations were computed by the method of reference 2 as given in reference 9. The calculations for the positive lift conditions are seen to be consistently higher than those for the negative lift coefficients.

It can be seen that the peak positive overpressures measured below the airplane are in closer agreement with the positive-lift-coefficient calculations, whereas those measured above the airplane are in closer agreement with the negative-lift-coefficient calculations. Such a result would be expected for airplane operating conditions in which lift effects are significant.

Wavelengths

From the time-interval data of figures 8 to 14 and from the accurate information on the positions and speed of the two airplanes, calculations have been made of wavelength, which is defined as the distance between the bow and tail waves. These wavelength values are shown in figures 8 to 14, are listed in table III, and are plotted in figure 17 as a function of distance. Also included in figure 17 is a curve calculated from equation (3) of reference 13, which is based on the far-field volume theory of reference 14. In general, the measured wavelength values are seen to be higher than the calculated values. Furthermore, the wavelengths measured above the airplane are definitely shorter than those measured below the airplane at comparable operating conditions. It can be seen that, in general, for comparable distances the data points corresponding to the higher pressures have the longer wavelengths. This result is in accord with observations made in reference 15. The trend of increasing wavelength with increasing distance from the generating airplane is similar to that predicted by the theory. The fact that the theory underestimates the wavelengths may possibly be due to the fact that the comparisons are made with the far-field theory and that lift effects are not accounted for.

Impulses

Positive and negative impulses for all the test flights have been obtained from integration of the records of figures 8 to 14 and from supplementary wavelength and time-interval information as included in table III. For data obtained below the generating airplane, the measured positive impulses were generally larger than the negative impulses. For data obtained above the airplane, however, the measured positive impulses were generally smaller than the negative impulses. It should be pointed out that in the integrations, the areas associated with the airplane wake (aft of the tail wave) were also included.

Correlation With Airplane Geometry

One of the main objectives of the tests was to obtain definite information relative to the way in which lift effects and volume effects combine in the generation of the shock-wave patterns from the generating airplane. The data of figure 18 have been reproduced from figures 10 and 12 to illustrate some of these findings. It was found in references 5, 7, and 16 that the shock-wave patterns beneath the airplane were closely related to the airplane geometry. In the present study, pressure signatures measured above and below the generating airplane have been adjusted in wavelength to conform to the length of the airplane and are compared with sketches showing the main components of the airplane.

Two general observations can be made. Some correlation exists between the locations of the individual shock waves and the geometrical features of the airplane. It is also obvious that the pressure signature measured above the airplane varies markedly from that measured below the airplane. In particular, the locations of the individual shock waves are different, and furthermore below the airplane the positive area exceeds the negative area whereas the reverse is true above the airplane.

SUMMARY OF RESULTS

In-flight probe measurements of the pressure field of a bomber airplane operating at Mach numbers from 1.42 to 1.69 have been made at distances of approximately 1,300 to 2,000 feet above and below the generating airplane and at distances of about 4,600 to 9,100 feet below. The results may be summarized as follows:

1. As distance from the airplane increases, the wavelength increases and the number of individual shock waves diminishes until the classical N-wave shape is approximated at a distance of 50 to 90 body lengths for the conditions of these tests.

2. The pressure waves measured below the airplane had higher peak positive values than those measured above the airplane at comparable distances. For data obtained below the airplane the measured positive impulses were generally larger than the negative impulses, whereas the reverse was true above the airplane. Such a result would be expected for airplane operating conditions in which lift effects are significant.

3. The combined lift-volume calculations for the far field are in good agreement with the pressure measurements made above and below the airplane.

Langley Research Center,
National Aeronautics and Space Administration,
Langley Station, Hampton, Va., July 5, 1963.

APPENDIX A

DESCRIPTION AND STATIC CALIBRATION OF PRESSURE INSTRUMENTATION

The instrumentation for measuring the pressure field about the bomber airplane consists of the following components: Two NASA model 49-TP inductance pressure gages (ref. 17) and a resistance-type temperature pickup mounted in the special probe on the fighter airplane as shown in figure 5; a carrier amplifier, an NASA recording oscillograph, a resistance-type temperature control box, and an NASA timer mounted in the rocket bay of the fighter airplane; and two solenoid valves and two constant-temperature chambers mounted in the nose bay. The pressure gage converts the static pressure on the probe into impedance changes which produce an unbalance on the inductance-resistance bridge. This output is amplified and demodulated in the carrier amplifier and recorded on film in the oscillograph.

The instrumentation necessary to measure this pressure field had to be suitable for flight environments. Also required was a high sensitivity and a frequency response that was flat from zero to 30 cps. To obtain the high sensitivity, a differential pressure gage was used. An absolute pressure gage, normally used to measure static-pressure changes, would not produce the required high sensitivity. When using a differential gage for this type of measurement, it is necessary to equalize the pressure on the gage during the time that the fighter airplane is climbing and descending. During the measuring period one side of the gage must be sealed off and used as a reference; this was accomplished by connecting one side of the gage to the reference orifice through a solenoid valve. Also connected in the reference side was a constant-temperature chamber. This added volume minimized changes in the reference pressure due to temperature changes caused by the aerodynamic heating of the long lengths of tubing that connected the reference orifice on the instrumented probe with the valve in the nose section. The volume of the tubing was about 1 percent of the chamber volume. To obtain the required frequency response, it was necessary to minimize the time lags by locating the measuring pressure gage very close to the orifice. The NASA type 49 gage was selected because of its high sensitivity, good acceleration characteristics, and very small size. Since its dimensions are only 1/4 by 7/16 by 7/16 inch, the gage could be mounted directly in the probe close to the orifice. All the other instrumentation was standard flight equipment.

It was decided to use two gages: gage 1, which measured the static pressure on the needle nose of the instrumented probe, and gage 2, which measured the static pressure on the body of the probe. (See figs. 4 and 5.) Gage 1 had a sensitivity of approximately 10 lb/sq ft per inch of film deflection and was recorded by a 100-cycle galvanometer. Gage 2 had a sensitivity of approximately 20 lb/sq ft per inch of film deflection and was recorded by a 50-cycle galvanometer. Once the reference valves are closed, the gages essentially become very sensitive altimeters. Gage 2 was used as a backup in case gage 1 was driven off scale by too large a change in altitude of the fighter airplane after the pilot had closed the reference valve. The lower frequency galvanometer was used to filter out any high-frequency noise that might occur.

The response of each measuring system was determined by the frequency response of the recording galvanometer. An example of this is shown in figure 19, where a step function was applied to the 50-cycle galvanometer and a step function was applied to the entire measuring system. It can be seen from these step functions that the response of both is the same. The time lag of the reference system was 3 seconds. This large lag limited the rate of climb and descent of the fighter airplane to 6,000 feet per minute and thus kept the gages and amplifiers from being overloaded.

The accuracy of the overall system was estimated to be 3 percent of the peak positive overpressures listed in table III. The hysteresis of the gage was 1 percent, and the accuracy of the galvanometers and amplifiers was 2 percent. The change in sensitivity of the gage was 6.5 percent per 100° F change in temperature. This was correctable to 1 percent by use of the resistance temperature gage. The effect of accelerating forces along the longitudinal axis of the fighter airplane (normal to the diaphragm) was 0.05 lb/sq ft per g. The system was constantly monitored by making static calibrations before and after each flight.

APPENDIX B

DESIGN AND AERODYNAMIC CALIBRATION OF PRESSURE PROBE

By Virgil S. Ritchie

DESIGN

Basic Considerations

The design of a flight probe for sensing static-pressure changes in the pressure field of a large disturbance-generating supersonic airplane involved a number of aerodynamic and structural considerations. A probe of conical shape and relatively large dimensions was considered suitable for a cantilever-type installation at the end of the nose boom of a probe airplane. The conical shape afforded the advantageous features of weak tip disturbance and thin boundary layer. The large dimensions afforded structural rigidity, suitable locations for miniature electrical pressure gages near the pressure-sensing orifices, and relatively large Reynolds numbers. The location of pressure gages near the sensing orifices reduced the possibility of pressure-lag errors. The large Reynolds numbers increased the likelihood of realizing a turbulent boundary layer on the probe without the use of artificial transition-fixing devices, which could introduce shock waves ahead of the pressure-sensing orifices. An arrangement of two small orifices circumferentially located in null-pressure regions about 75° apart afforded some reduction of the errors associated with changes of flow angularity (crossflow) around the conical probe. This asymmetric arrangement necessitated probe orientations with the pressure orifices facing the incident disturbance wave to be measured, but it was considered superior to a symmetrical arrangement of orifices distributed around the circumference of the probe. The asymmetric arrangement was employed for a primary system of pressure orifices located in the conical tip portion of the probe and for a secondary system of orifices located in an enlarged conical region of the probe. For the latter system of orifices, which was employed to supplement the primary system, suitable calibration information was required, because of likely effects of the probe-enlargement shock wave as well as the thicker boundary layer at the secondary location.

Present Application

Principal details of the flight probe and its installation on the nose boom of a "century series" supersonic airplane are shown in figures 4 and 5. This probe employed six pressure-sensing systems including the two systems for indicating disturbance-related pressure changes, two systems for providing reference pressures for the differential-pressure gages, and systems for providing approximate free-stream static (ambient) pressure and pitot pressure for the airplane flight instruments. The orifices and the tube for providing approximate ambient and pitot pressures for the flight instruments were located at the bottom of the probe for all flights. The forward end of the probe was made rotatable in order to facilitate the required orientation with disturbance-sensing orifices facing

the incident disturbance waves from the generating airplane. The rear portion of the probe was secured to the nose boom in such a manner that the angle of attack of the probe would be near 0° for the expected flight conditions. The miniature pressure gages in the probe were installed with their diaphragms perpendicular to the longitudinal axis of the probe in order to minimize possible effects of lateral accelerations.

WIND-TUNNEL TESTS

Introduction

Early evidence concerning the reflection characteristics of the probe was obtained from unreported preliminary tests of a 0.75-scale model of the flight probe in the Langley 4- by 4-foot supersonic pressure tunnel at a Mach number of about 1.82. The average test Reynolds number (per foot) was about 2.6×10^6, and the average static pressure corresponded to a pressure altitude of about 50,000 feet for standard atmospheric conditions. These tests involved the streamwise movement of the probe (with natural transition) across a disturbance (bow wave) generated by a body of revolution and the measurement of probe-sensed pressure changes in the vicinity of the disturbance. These early tests indicated that the primary system of orifices of the probe sensed the same maximum pressure changes (across the employed shock wave) that were estimated by theoretical methods, whereas the secondary system of orifices sensed pressure changes about 10 percent larger than the estimated values. Also, the probe-sensed pressure changes in the vicinity of the disturbance appeared to be of the type generally associated with turbulent boundary layers (ref. 18). On the basis of this early information, the full-scale flight probe was constructed and in-flight measurements were undertaken with the view of investigating the reflection characteristics of the flight probe by means of wind-tunnel tests at a later date.

Accordingly, after in-flight measurements, tests of the flight probe were conducted in the Langley 4- by 4-foot supersonic pressure tunnel to calibrate the approximate reflection characteristics of the probe at a Mach number near those employed for the in-flight measurements. The probe reflection characteristics were largely determined by the same procedure as that employed for the early tests at a Mach number of 1.82. This procedure involved streamwise movement of the probe across a weak axisymmetrical shock wave of predetermined strength and the measurement of probe-indicated pressure changes across the disturbance.

Unreported additional tests of the full-scale probe across weak shock waves in the Langley 4- by 4-foot supersonic pressure tunnel provided information concerning the effects of angle of attack on probe reflection characteristics. Although these tests have not been included in the present report, the results were used in arriving at the approximate reflection factors reported subsequently in this appendix.

Symbols

M_∞	free-stream Mach number
p_1	static pressure sensed by primary system of orifices (location 1), lb/sq ft
p_2	static pressure sensed by secondary system of orifices (location 2), lb/sq ft
p_3	static pressure sensed by system of orifices (location 3) providing static pressure for probe-airplane flight instruments, lb/sq ft
$p_{1,ref}$	static pressure sensed by orifices providing reference pressure for gage 1, lb/sq ft
$p_{2,ref}$	static pressure sensed by orifices providing reference pressure for gage 2, lb/sq ft
p_t	total pressure, lb/sq ft
p_t'	pitot pressure, lb/sq ft
p_∞	free-stream static pressure, lb/sq ft
Δp	peak or maximum pressure change across oblique shock, lb/sq ft
r	radius of body of revolution, in.
x	axial distance from nose of body of revolution, in.
x_s	approximate longitudinal (streamwise) distance from mean location of oblique shock (bow wave), positive when orifices are rearward of shock, in.
y	approximate separation distance (perpendicular to airflow direction) between disturbance-generating body and pressure-sensing probe or instrument, in.
α	angle of attack of probe, deg

Apparatus and Tests

Test facility and conditions.- The present calibration tests were conducted in the Langley 4- by 4-foot supersonic pressure tunnel at a Mach number of about 2.01 (slightly larger than the average probe-airplane Mach number of about 1.95 employed for in-flight measurements). The average Reynolds number per foot for these tests was about 2.4×10^6, whereas the Reynolds numbers per foot for in-flight measurements ranged from about 1.8×10^6 to 4.5×10^6. The free-stream

static pressure employed for the tests corresponded to a pressure altitude of about 55,000 feet for standard atmospheric conditions.

Test apparatus and procedures.- The arrangement illustrated at the top of figure 20 was used in the calibration of the flight probe at various angles of attack. This arrangement, involving the location of all static-pressure orifices and the pitot-pressure tube on the bottom of the probe, corresponded to that employed for the probe-airplane flights over the generating airplane. Conical tip 1 (see fig. 5) was used on the probe for the calibration tests.

The apparatus and arrangements for generating an oblique shock wave and for surveys to determine the strength of this shock are illustrated in figure 21. The procedure employed for surveys in the vicinity of the shock was to move the survey instrument in the streamwise direction and measure the pressures at sufficiently close intervals to define the maximum change of pressure across the shock. Two different methods, one involving a pitot-tube technique and the other a static-pressure orifice on a plate, gave identical results in defining the maximum pressure changes. This oblique shock wave of predetermined strength afforded a means for determining the reflection characteristics of the probe.

Measurements.- Absolute manometers were used for measuring tunnel total pressures as well as reference static pressures and pitot pressures in the test section. Differential-pressure gages with ranges of 0.25 and 0.5 pound per square foot were employed for measuring differences between the reference static pressure and the various local static pressures sensed by the probe or the survey instrument. A gage with a range of 1 pound per square foot was used for measuring differences between the reference pitot pressure and local pitot pressures sensed by the survey instrument. Gages with ranges of 3 and 8 pounds per square foot were used for measuring differences between the total pressure in the tunnel and the pitot pressure sensed by the flight probe. All gages were calibrated before and after the wind-tunnel tests.

Data and Precision

Probe calibration.- Most of the calibration data shown in figure 20 represent averages of measurements from two separate tests. The static-pressure data are expressed in the form of ratios of local probe-sensed static pressures to local free-stream static pressures in order to minimize possible errors associated with flow nonuniformities. Random errors in measurements during probe-calibration and tunnel-calibration tests are believed to influence the static-pressure ratios, as well as the ratios of pitot to total pressure, by no more than about ± 0.005.

Pressure measurements in vicinity of oblique shock wave.- Probe-indicated static pressures in the vicinity of the body-generated oblique shock (bow wave) are expressed as ratios of probe-indicated static pressure to an average (not local) free-stream static pressure. Although these ratios are influenced by random errors in measurements in the same manner as the probe-calibration data, the possible errors in measuring pressure changes across the oblique shock wave are considerably less than ± 0.005. The survey technique appears to reduce random errors in measurement to less than about 0.15 percent of the free-stream static

pressure or to less than about 3.5 percent of average pressure changes across the shock wave. An experimental measurement-repeatability check, involving several traverses of the probe across the oblique shock wave, indicated scatter of less than ±2 percent in the shock-wave pressure changes sensed by the primary orifices or by the secondary orifices.

Results and Discussion

Probe calibration at angles of attack.- Calibration tests of the probe at various angles of attack yielded the results shown in figure 20. The primary system of orifices and the reference-pressure orifices in the conical tip portion of the probe indicated pressures which were generally about 1 percent larger than the free-stream static pressure. These cone-surface pressures were sufficiently influenced by angle-of-attack changes to make the primary pressure-sensing arrangement fairly sensitive to small changes in crossflow such as might be introduced by turbulence, probe oscillations, and flow-angularity changes across shock waves, that might occur in flight. The sensitivity of alternate conical tip 2 to angle-of-attack effects was not determined from calibration tests, but the slightly different circumferential spacings of orifices in tips 1 and 2 (fig. 5) suggest that angle-of-attack effects might be somewhat larger for tip 2 than for tip 1.

The secondary system of orifices and the reference-pressure orifices located in the conical portion of the probe behind the enlargement region indicated pressures 2 or 3 percent less than free-stream static pressure. These pressures were not influenced as much by angle-of-attack changes as were the pressures sensed by the two systems of orifices in the conical tip of the probe.

The orifice system for the flight instruments indicated pressures about 1 or 2 percent less than free-stream static pressure. These pressures were influenced more by angle-of-attack changes than were the pressures indicated by the other orifice systems. This increased influence of angle of attack was largely associated with the size and location of the orifices for the flight-instrument system.

The pitot pressures sensed by the tube that was offset from the bottom of the probe were somewhat larger than those expected for a tube located ahead of the interference field of the probe. The probe-indicated pitot pressures varied consistently with angle-of-attack changes.

Probe capability for sensing pressure changes across an oblique shock wave.- Figure 22(a) illustrates the approximate capability of the probe, at an angle of attack of 0°, for sensing pressures in the vicinity of a weak shock wave. It is seen that the primary system of orifices in the conical tip senses such pressure changes with small error, whereas the secondary system of orifices senses pressure changes considerably larger than the estimated changes. These indicated probe capabilities are supplemented by the data in figure 22(b), which compares probe-indicated, survey-indicated, and estimated maximum pressure changes across the oblique shock wave.

Correlation of these indicated characteristics of the flight probe at an angle of attack of 0° and a Mach number of 2.01 with unreported characteristics of a 0.75-scale model of the flight probe at an angle of attack of 0° and a Mach number of 1.82 indicated that the primary system of orifices is capable of accurately sensing maximum or peak pressure changes across weak shock waves at these Mach numbers. This correlation also indicated that the secondary system of orifices sensed pressure rises that were too large by about 10 percent at a Mach number of 1.82 and about 30 percent at a Mach number of 2.01.

Unreported tests of the flight probe in the vicinity of an oblique shock wave at a Mach number of 2.01 indicated that reflection characteristics of the probe at angles of attack of 1° and -1° were somewhat different from those at an angle of attack of 0°. Such differences were larger for the secondary system of orifices than for the primary system.

The described probe capabilities, as obtained from wind-tunnel tests, are believed to be representative of in-flight probe capabilities at comparable Mach numbers, Reynolds numbers, and angles of attack. Possible differences in turbulence and boundary-layer transition are believed to be the principal sources of any discrepancies between probe characteristics in the wind tunnel and in flight.

Probe reflection factors for correcting in-flight measurements.- On the basis of the available information, a reflection factor of 1.00 appeared to be appropriate for the primary system of orifices at Mach numbers near 1.82 and 2.01 and angles of attack near 0°. The reported probe-airplane Mach numbers employed for in-flight measurements were between 1.85 and 1.99. The estimated probe angles of attack for in-flight measurements ranged from -0.4° to -1.5° (not including likely changes as the probe airplane traversed the disturbance field of the generating airplane). These negative angles of attack could possibly change the reflection factor by several percent. Angle-of-attack corrections have not been applied to the in-flight pressure measurements obtained from the primary system of orifices.

Reflection factors for the secondary system of orifices appeared to vary with Mach number, probe angle of attack, and strength of the incident disturbance wave. Applicable reflection factors for in-flight measurements obtained from the secondary system of orifices could not be accurately determined from the available information, but the following values are believed to be reliable within about 10 percent:

Flight	Approximate reflection factor for secondary system
1	1.23
2	1.16
3	1.15
4	1.07
5	1.12
6	1.17
7	1.13

The reported values of in-flight pressure data were obtained by dividing the actual measurements by these reflection factors.

General comments.- The supersonic wind-tunnel tests of the probe designed for in-flight measurements yielded the following indications of probe capability for sensing pressure changes across weak disturbances:

(1) The primary system of orifices located in the conical tip portion of the probe appeared to be capable of accurately sensing the maximum or peak changes of static pressure across weak shock waves at Mach numbers near 1.82 and 2.01 when the probe axis was alined with the direction of flight or relative free-stream airflow ($\alpha = 0^{\circ}$). The reflection characteristics of the probe were influenced somewhat by small changes of angle of attack.

(2) The secondary system of orifices located in an enlarged conical portion of the probe indicated shock-proximity pressure changes somewhat larger than those obtained by special surveys and by theoretical estimates. Approximate reflection factors for the conditions of the in-flight measurements varied from about 1.07 to about 1.23.

REFERENCES

1. Whitham, G. B.: The Flow Pattern of a Supersonic Projectile. Communications on Pure and Appl. Math., vol. V, no. 3, Aug. 1952, pp. 301-348.

2. Walkden, F.: The Shock Pattern of a Wing-Body Combination, Far From the Flight Path. Aero. Quarterly, vol. IX, pt. 2, May 1958, pp. 164-194.

3. Morris, John: An Investigation of Lifting Effects on the Intensity of Sonic Booms. Jour. R.A.S., vol. 64, no. 598, Oct. 1960, pp. 610-616.

4. Crosthwait, E. L.: Sonic Boom Theory and the B-58. Rep. No. FZA-4-405, CONVAIR, Apr. 28, 1961.

5. Mullens, Marshall E.: A Flight Test Investigation of the Sonic Boom. AFFTC-TN-56-20, Air Res. and Dev. Command, U.S. Air Force, May 1956.

6. Smith, Harriet J.: Experimental and Calculated Flow Fields Produced by Airplanes Flying at Supersonic Speeds. NASA TN D-621, 1960.

7. Maglieri, Domenic J., Huckel, Vera, and Parrott, Tony L.: Ground Measurements of Shock-Wave Pressure for Fighter Airplanes Flying at Very Low Altitudes and Comments on Associated Response Phenomena. NASA TM X-611, 1961.

8. Carlson, Harry W.: An Investigation of Some Aspects of the Sonic Boom By Means of Wind-Tunnel Measurements of Pressures About Several Bodies at a a Mach Number of 2.01. NASA TN D-161, 1959.

9. Carlson, Harry W.: An Investigation of the Influence of Lift on Sonic-Boom Intensity By Means of Wind-Tunnel Measurements of the Pressure Fields of Several Wing-Body Combinations at a Mach Number of 2.01. NASA TN D-881, 1961.

10. Carlson, Harry W.: Wind-Tunnel Measurements of the Sonic-Boom Characteristics of a Supersonic Bomber Model and a Correlation With Flight-Test Ground Measurements. NASA TM X-700, 1962.

11. Ryhming, I. L., and Yoler, Y. A.: Supersonic Boom of Wing-Body Configurations. Jour. Aerospace Sci., vol. 28, no. 4, Apr. 1961, pp. 313-320.

12. Ryhming, I. L.: The Supersonic Boom of a Projectile Related to Drag and Volume. Jour. Aerospace Sci., vol. 28, no. 2, Feb. 1961, pp. 113-118, 157.

13. Maglieri, Domenic J., Hubbard, Harvey H., and Lansing, Donald L.: Ground Measurements of the Shock-Wave Noise From Airplanes in Level Flight at Mach Numbers to 1.4 and at Altitudes to 45,000 Feet. NASA TN D-48, 1959.

14. Whitham, G. B.: The Behaviour of Supersonic Flow Past a Body of Revolution, Far From the Axis. Proc. Roy. Soc. (London), ser. A, vol. 201, no. 1064, Mar. 7, 1950, pp. 89-109.

15. DuMond, Jesse W. M., Cohen, E. Richard, Panofsky, W. K. H., and Deeds, Edward: A Determination of the Wave Forms and Laws of Propagation and Dissipation of Ballistic Shock Waves. J. Acous. Soc. of America, vol. 18, no. 1, July 1946, pp. 97-118.

16. Hubbard, Harvey H., Maglieri, Domenic J., Huckel, Vera, and Hilton, David A.: Ground Measurements of Sonic-Boom Pressures for the Altitude Range of 10,000 to 75,000 Feet. NASA TM X-633, 1962.

17. Patterson, John L.: A Miniature Electrical Pressure Gage Utilizing a Stretched Flat Diaphragm. NACA TN 2659, 1952.

18. Liepmann, H. W., Roshko, A., and Dhawan, S.: On Reflection of Shock Waves From Boundary Layers. NACA Rep. 1100, 1952. (Supersedes NACA TN 2334.)

TABLE I.- SUMMARY OF FLIGHT CONDITIONS

Flight	Generating airplane (bomber)						Probe airplane (fighter)				ΔM	ΔV, ft/sec	Vertical separation distance, Δh, ft	Horizontal separation distance, Δs, ft	y, ft
	Altitude, h, ft	M	True heading, deg	Ground velocity, V, ft/sec	Gross weight, W, lb	Calculated, C_L	Altitude, h, ft	M	True heading, deg	Ground velocity, V, ft/sec					
1	48,400	1.57	267	1,410	115,000	0.192	47,060	1.98	267	1,790	0.41	380	1,340	200	1,355
2	47,455	1.42	268	1,266	116,400	.230	45,850	1.91	269	1,724	.49	458	1,605	280	1,630
3	39,980	1.65	269	1,500	83,750	.083	38,333	1.97	269	1,842	.32	342	1,647	160	1,654
4	48,440	1.61	264	1,430	115,200	.187	50,110	1.85	265	1,655	.24	225	-1,670	720	-1,820
5	40,600	1.69	268	1,472	82,700	.087	42,580	1.95	266	1,725	.26	232	-1,980	230	-1,994
6	48,270	1.68	269	1,501	113,000	.165	39,190	1.99	267	1,801	.31	300	9,080	1,070	9,155
7	40,710	1.69	264	1,525	84,000	.083	36,115	1.96	262	1,805	.27	280	4,595	400	4,615

TABLE II.- SUMMARY OF WEATHER DATA

Flight	Altitude, h, ft	Atmospheric pressure, lb/sq ft	Temperature, °F	Wind components, fps		
				Headwind	From port	From starboard
1	46,000	301	-78	111	--	12
	47,000	288	-79	101	--	5
	48,000	274	-80	88	--	5
	49,000	259	-81	79	--	4
	50,000	249	-81	81	--	4
2	44,000	324	-78	73	--	54
	45,000	309	-81	77	--	48
	46,000	293	-82	87	--	55
	47,000	280	-80	97	--	61
	48,000	265	-77	93	--	58
	49,000	253	-75	87	--	55
3	37,000	458	-76	38	--	117
	38,000	437	-77	41	--	127
	39,000	414	-78	69	--	130
	40,000	393	-80	73	--	117
	41,000	374	-79	76	--	108
4	47,000	290	-85	99	46	---
	48,000	276	-86	93	44	---
	49,000	259	-87	90	42	---
	50,000	249	-86	90	34	---
	51,000	236	-85	89	26	---
5	39,000	432	-70	128	68	---
	40,000	412	-78	133	72	---
	41,000	391	-82	133	72	---
	42,000	368	-84	118	63	---
	43,000	351	-87	106	56	---
	44,000	334	-91	109	58	---
6	38,000	455	-74	102	14	---
	39,000	432	-77	104	15	---
	40,000	412	-79	103	9	---
	41,000	389	-82	100	0	---
	42,000	370	-84	98	--	2
	43,000	353	-85	96	8	---
	44,000	334	-85	95	17	---
	45,000	318	-86	95	24	---
	46,000	303	-85	96	31	---
	47,000	288	-83	95	31	---
	48,000	276	-84	92	30	---
	49,000	261	-87	92	30	---
	50,000	249	-87	93	30	---
7	35,000	522	-62	88	6	---
	36,000	499	-66	93	6	---
	37,000	474	-70	99	7	---
	38,000	455	-74	103	7	---
	39,000	432	-77	104	7	---
	40,000	412	-79	103	2	---
	41,000	389	-82	99	7	---
	42,000	370	-84	98	--	9

TABLE III.- SUMMARY OF MEASURED PEAK POSITIVE OVERPRESSURES,

IMPULSES, SIGNATURE LENGTHS, AND TIME INTERVALS

Flight	Bomber		Fighter	y, ft	Measured							
					Gage 1			Gage 2			X, ft	Δt, sec
	M	Altitude, h, ft	Altitude, h, ft		Δp, lb/sq ft	I_{pos}, $\frac{\text{lb-sec}}{\text{sq ft}}$	I_{neg}, $\frac{\text{lb-sec}}{\text{sq ft}}$	Δp, lb/sq ft	I_{pos}, $\frac{\text{lb-sec}}{\text{sq ft}}$	I_{neg}, $\frac{\text{lb-sec}}{\text{sq ft}}$		
1	1.57	48,400	47,060	1,355	3.90	0.134	0.099	4.06	0.148	0.081	157	0.110
2	1.42	47,455	45,850	1,630	3.35	.122	.044	3.46	.092	.058	129	.102
3	1.65	39,980	38,333	1,654	4.00	-----	-----	3.75	.104	.061	143	.096
4	1.61	48,440	50,110	-1,820	1.72	.042	.051	1.55	.037	.036	123	.086
5	1.69	40,600	42,580	-1,994	2.41	.045	.074	2.05	.041	.056	127	.086
6	1.68	48,270	39,190	9,155	1.31	.048	.034	1.24	.047	.024	222	.148
7	1.69	40,710	36,115	4,615	-----	-----	-----	2.14	.061	.037	161	.105

L-63-4710

Figure 1.- Photograph of delta-wing supersonic bomber used as the generating airplane in the present investigation. (Courtesy U.S. Air Force.)

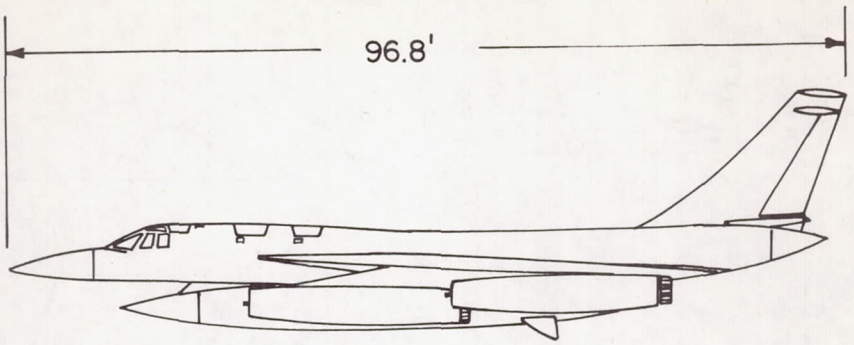

(a) Profile view.

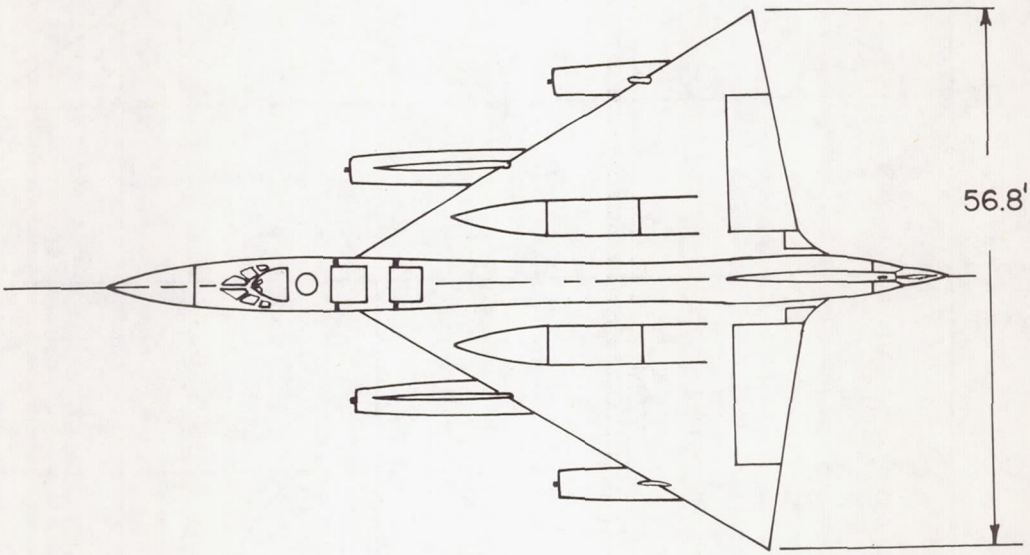

(b) Plan view.

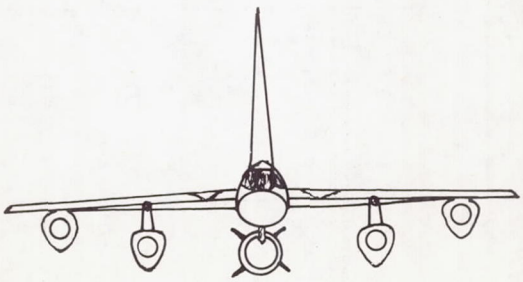

(c) Front view.

Figure 2.- Three-view schematic diagram of delta-wing bomber airplane used for the in-flight probe tests. Total wing area, 1,542 square feet.

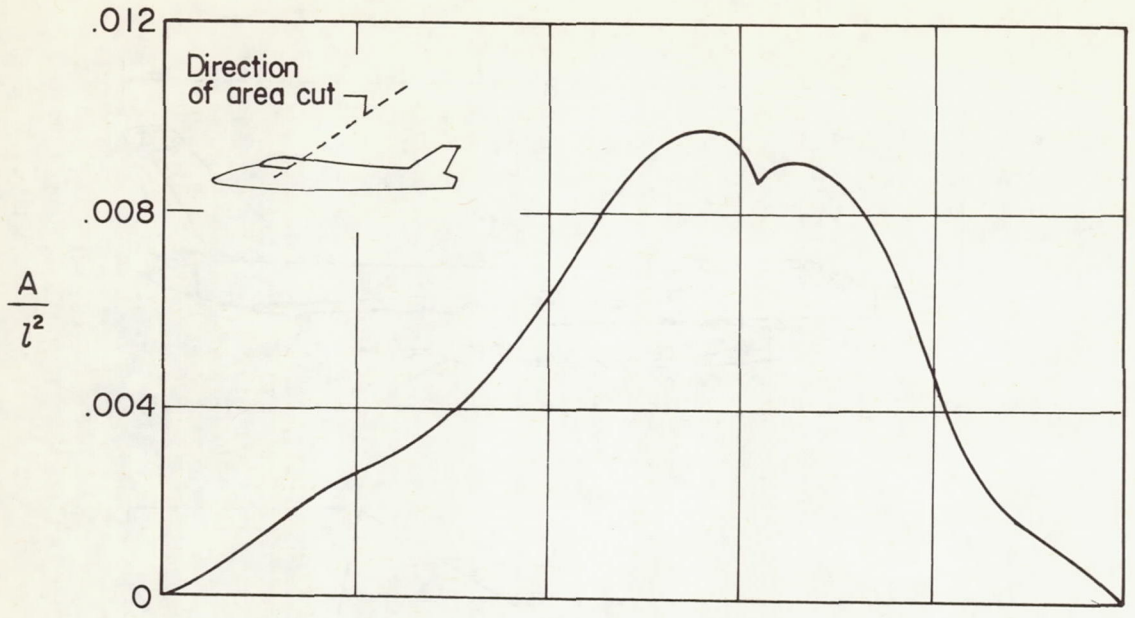

(a) Area distribution based on oblique cuts for positions above the airplane.

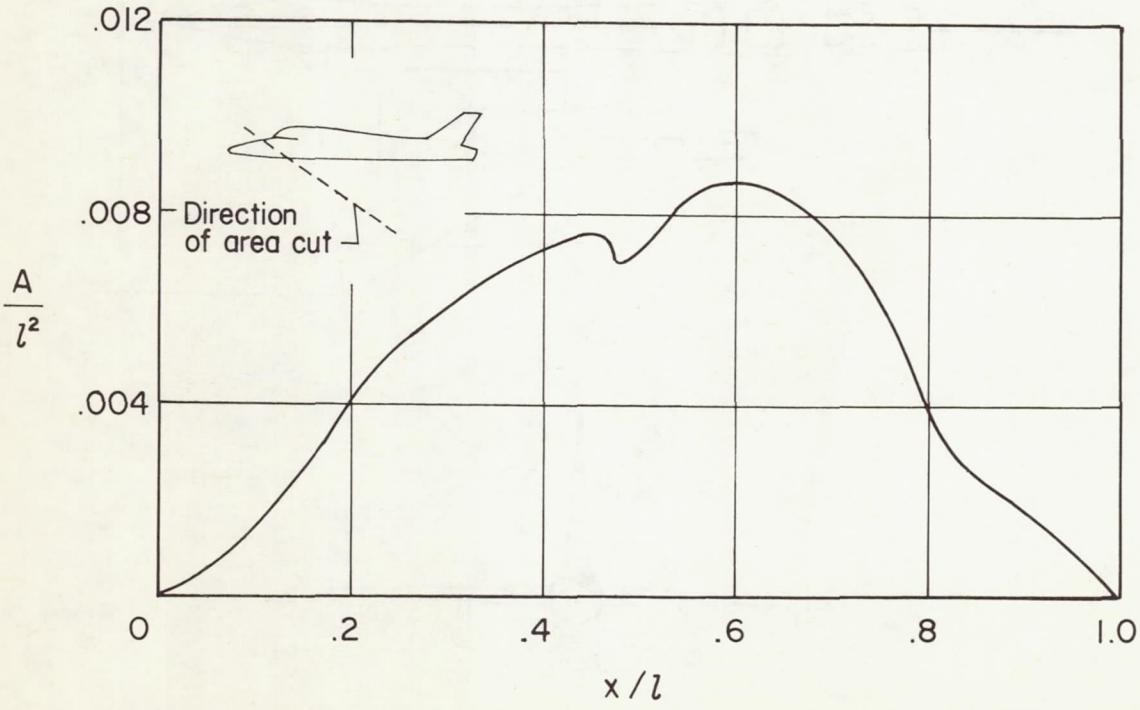

(b) Area distribution based on oblique cuts for positions below the airplane.

Figure 3.- Area distributions of delta-wing bomber used as generating airplane (no wake effects included). Oblique cuts; M = 1.65.

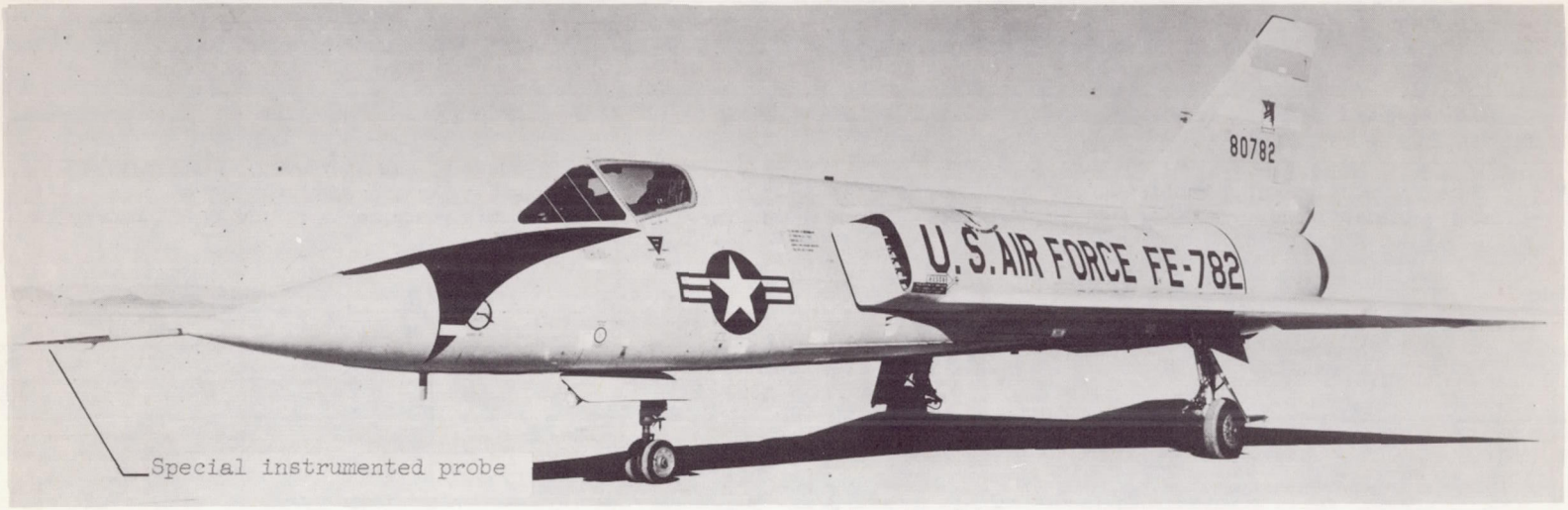

(a) Probe airplane. (Courtesy U.S. Air Force.)

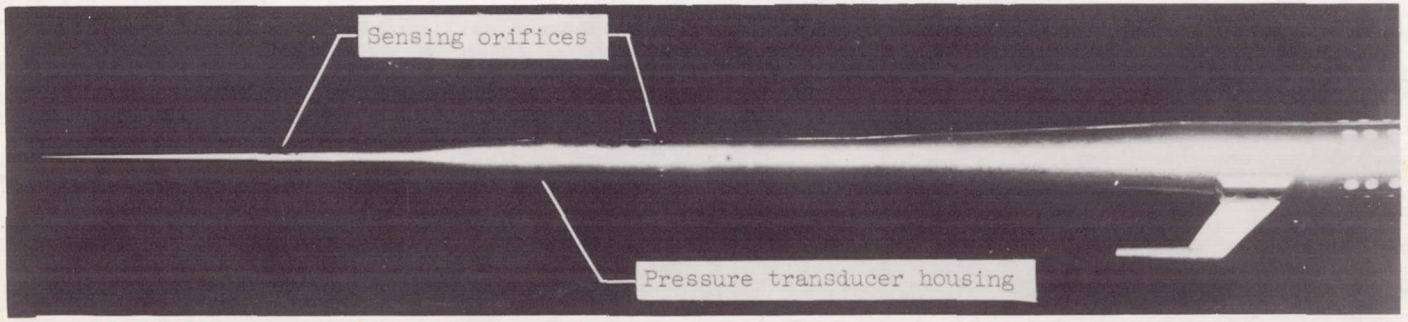

(b) Probe used for in-flight pressure measurements. L-63-4711

Figure 4.- Fighter airplane used with nose-boom probe installation for measuring the pressure field in the vicinity of the disturbance-generating airplane.

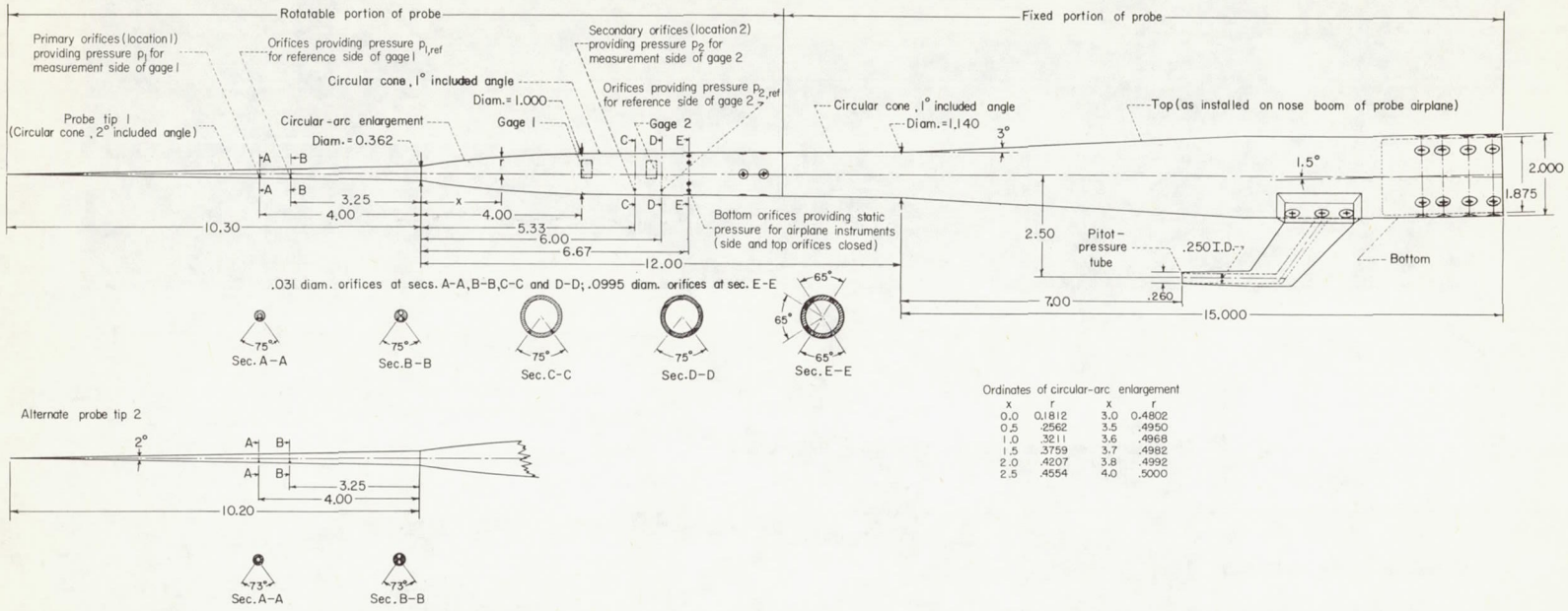

Ordinates of circular-arc enlargement

x	r	x	r
0.0	0.1812	3.0	0.4802
0.5	.2562	3.5	.4950
1.0	.3211	3.6	.4968
1.5	.3759	3.7	.4982
2.0	.4207	3.8	.4992
2.5	.4554	4.0	.5000

Figure 5.- Principal details and dimensions of full-scale probe used for in-flight measurements and for wind-tunnel tests at a Mach number of about 2.01. (Rotatable portion of probe is positioned for probe-airplane flight over generating airplane.) Dimensions are in inches.

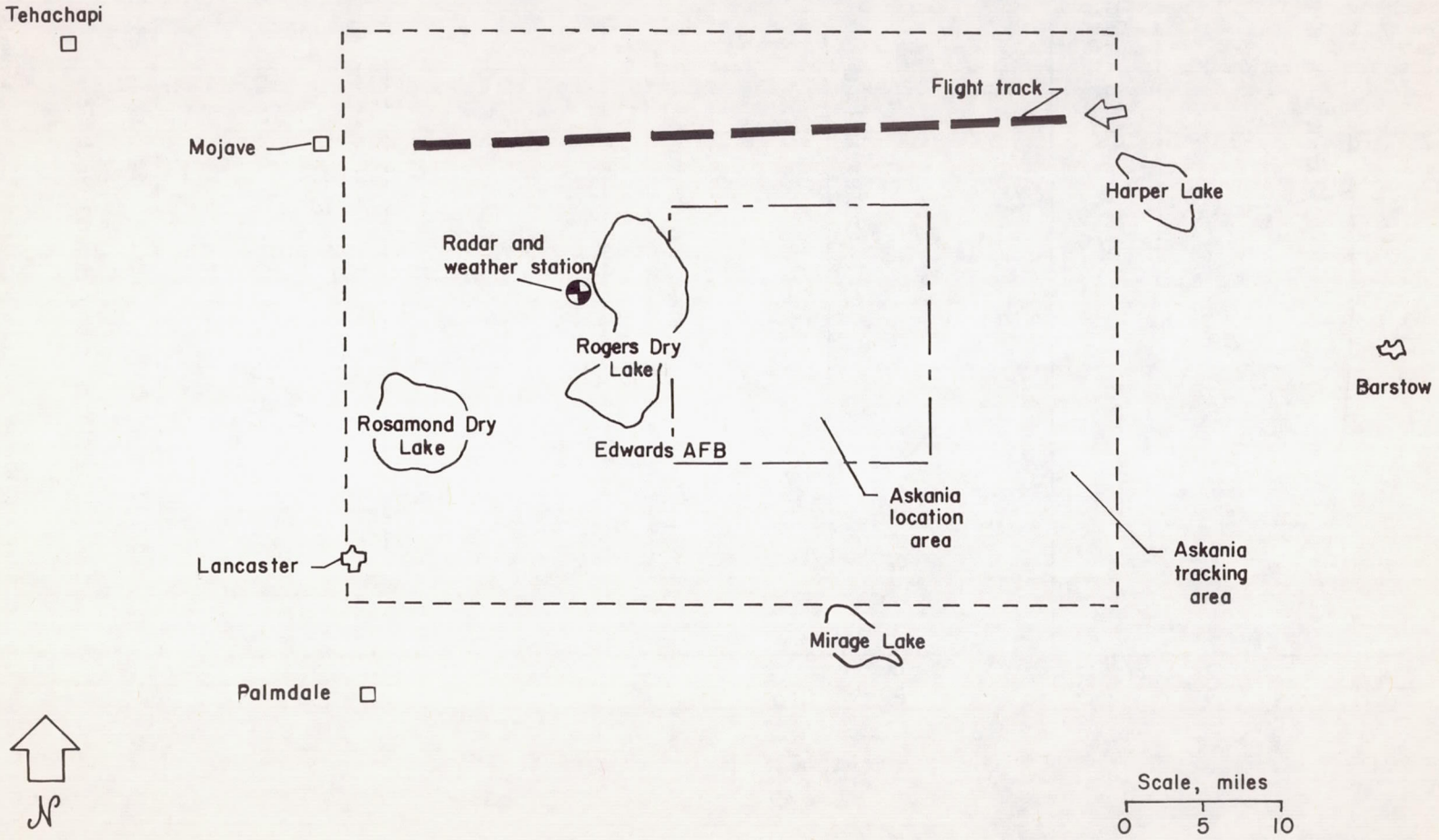

Figure 6.- Schematic view of test area showing location and direction of airplane flight track and locations of tracking network and weather stations.

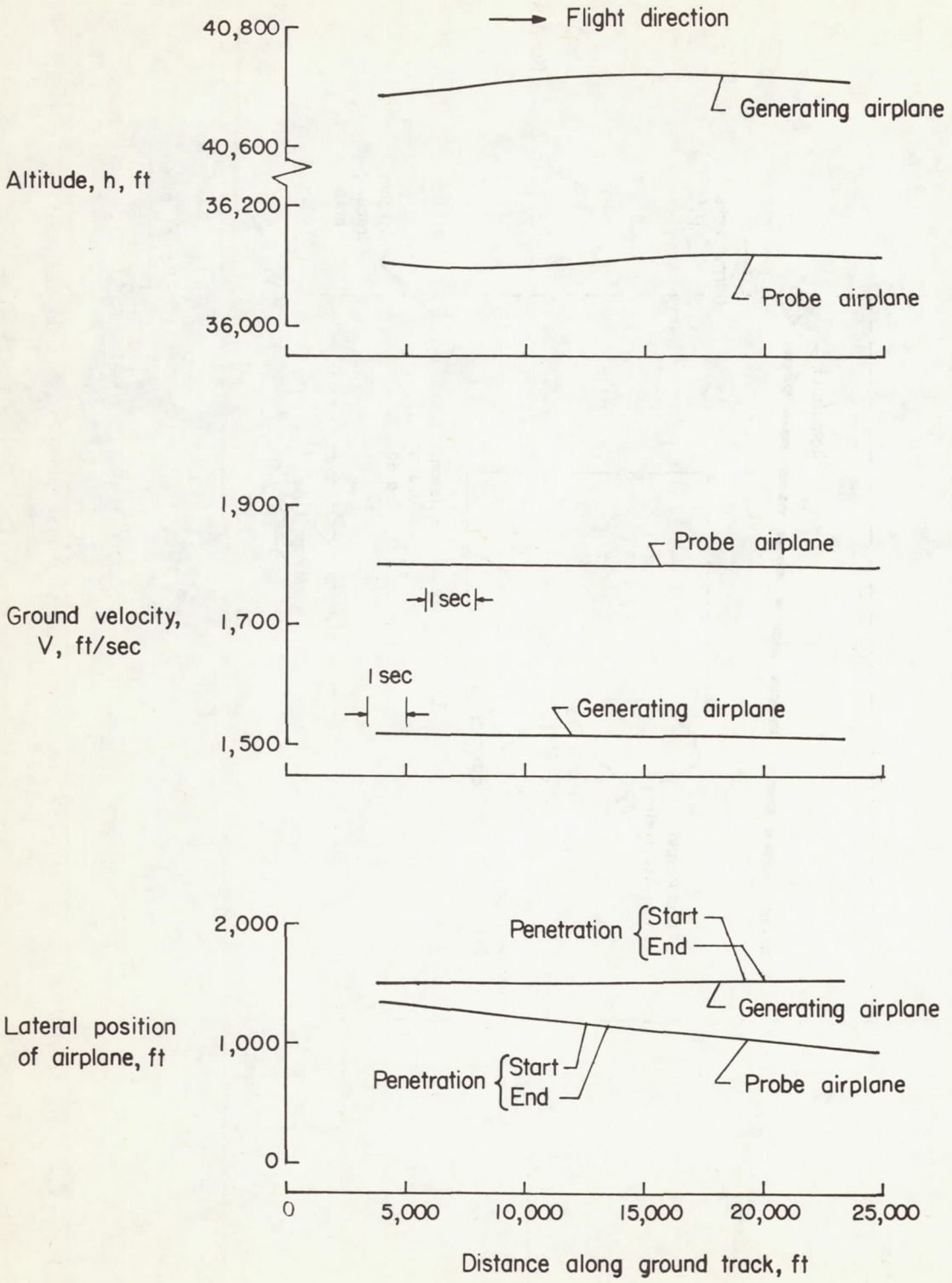

Figure 7.- Typical altitudes, velocities, and lateral positions of generating and probe airplanes as obtained from Askania data (flight 7).

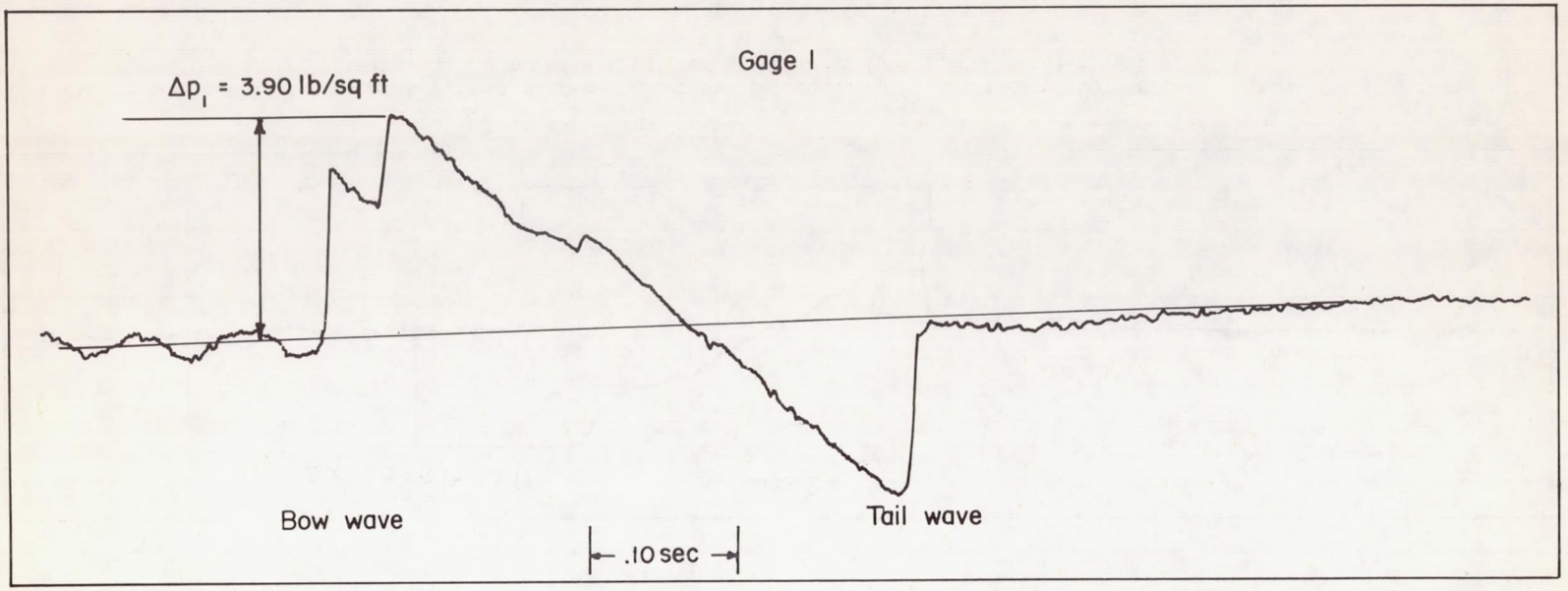

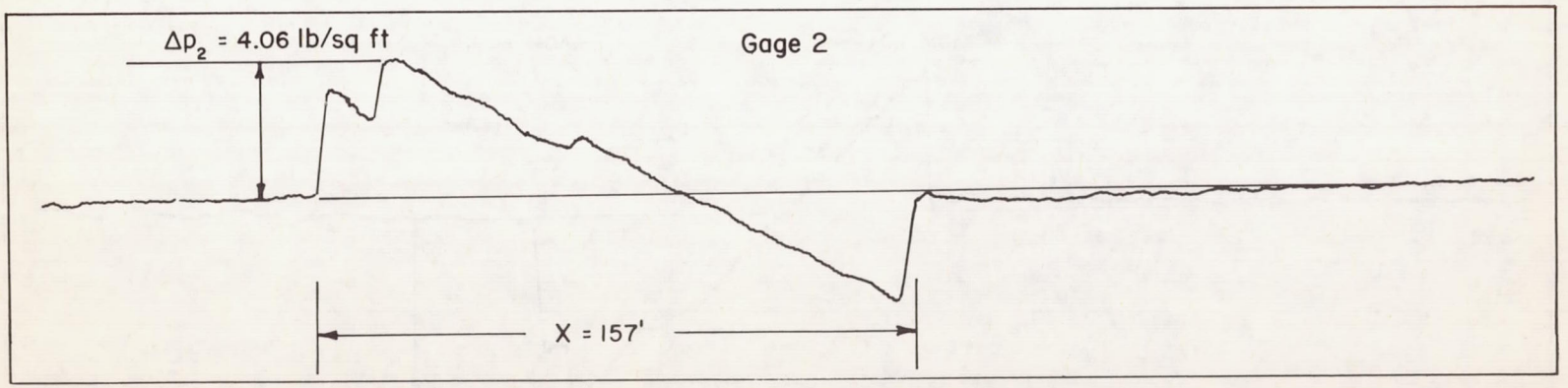

Figure 8.- In-flight time histories of differential pressures measured at altitude of 47,060 feet in flow field of bomber airplane flying at altitude of 48,400 feet (y = 1,355 feet); flight 1.

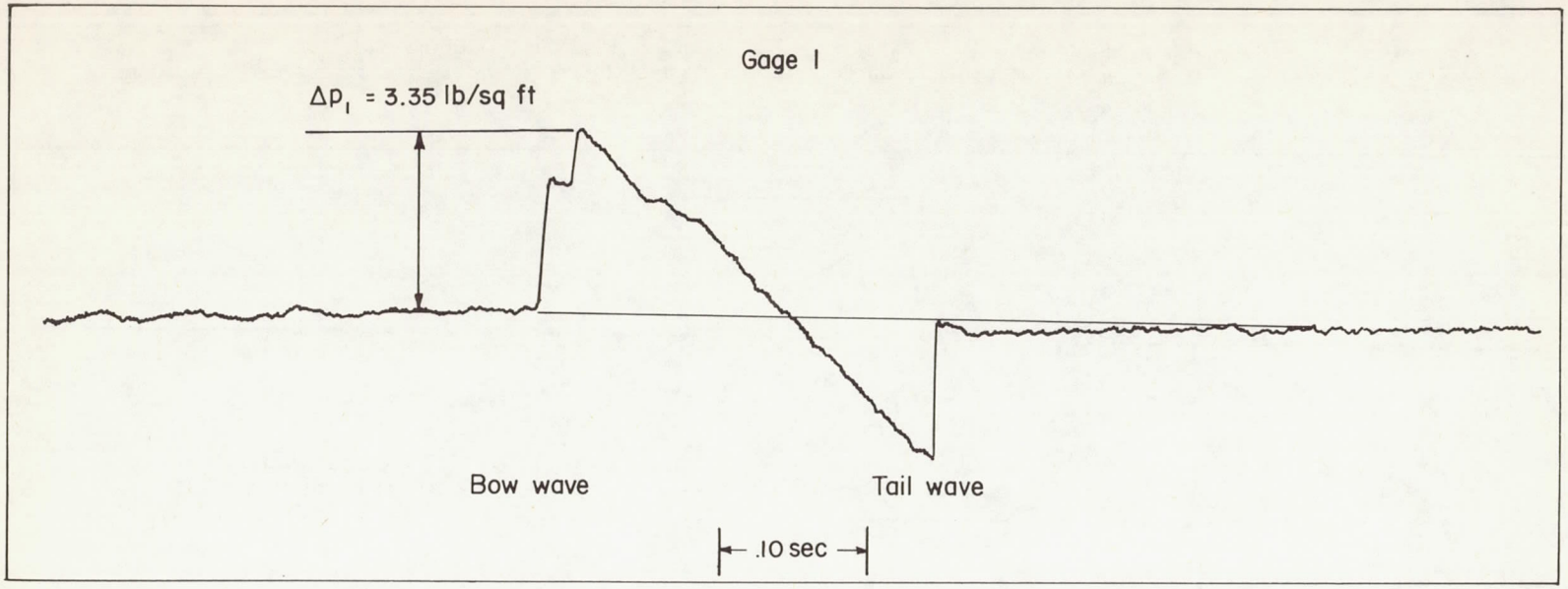

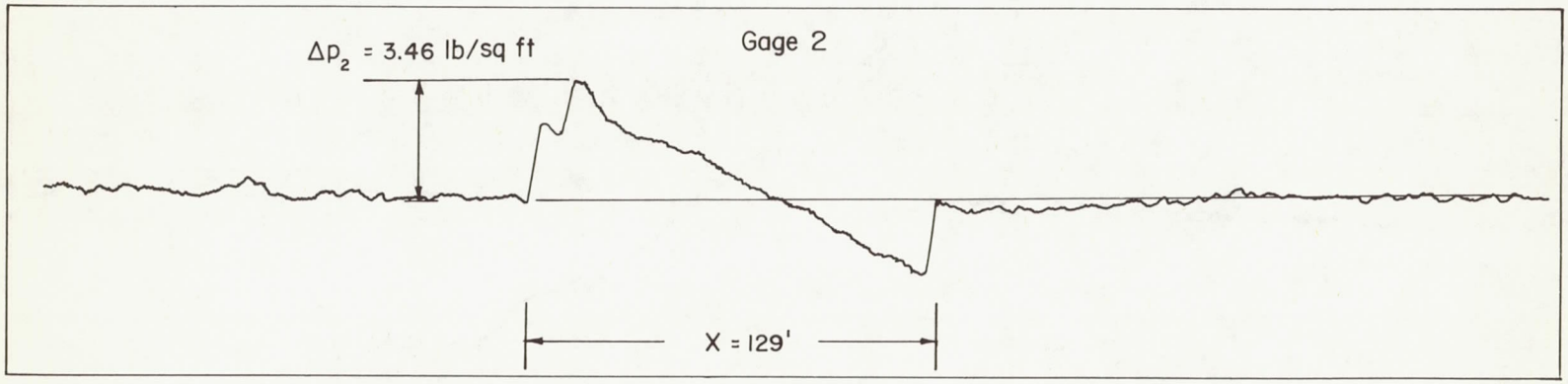

Figure 9.- In-flight time histories of differential pressures measured at altitude of 45,850 feet in flow field of bomber airplane flying at altitude of 47,455 feet (y = 1,630 feet); flight 2.

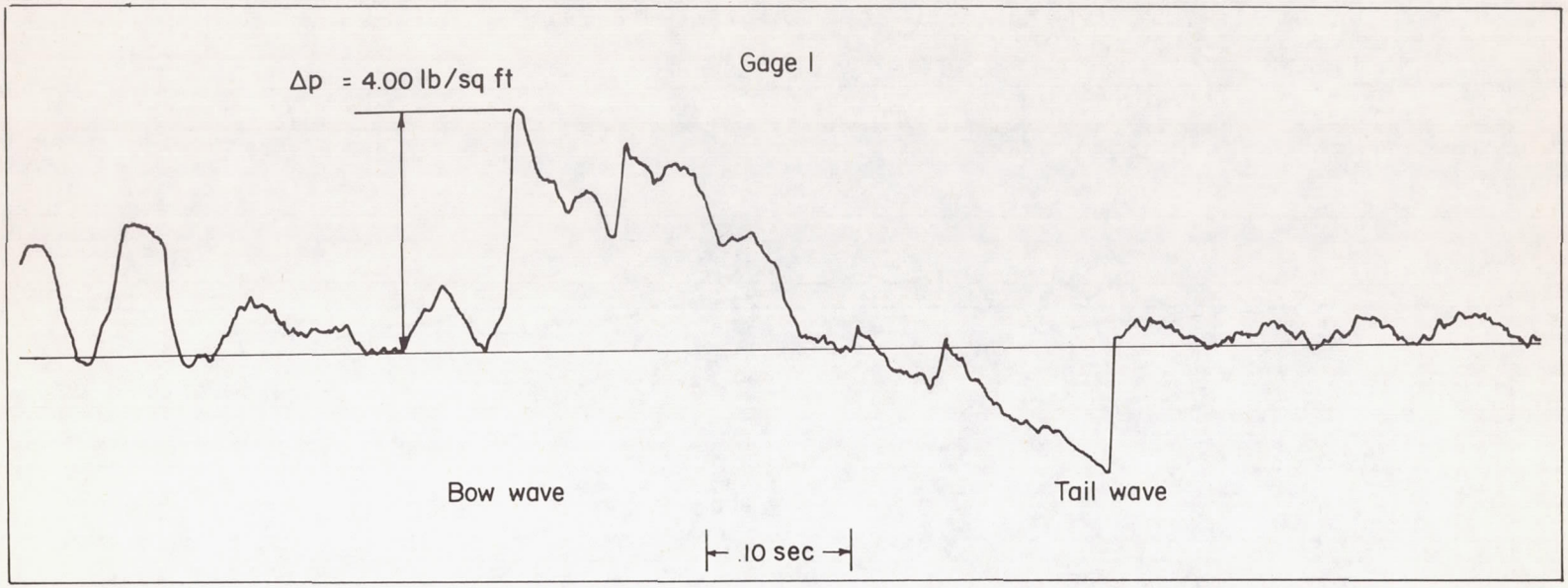

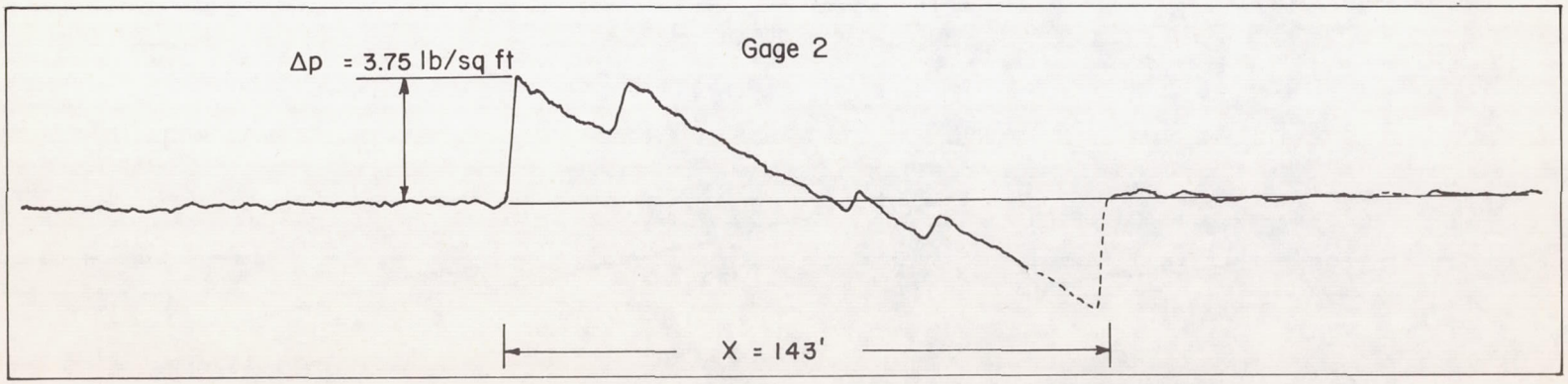

Figure 10.- In-flight time histories of differential pressures measured at altitude of 38,333 feet in flow field of bomber airplane flying at altitude of 39,980 feet (y = 1,654 feet); flight 3.

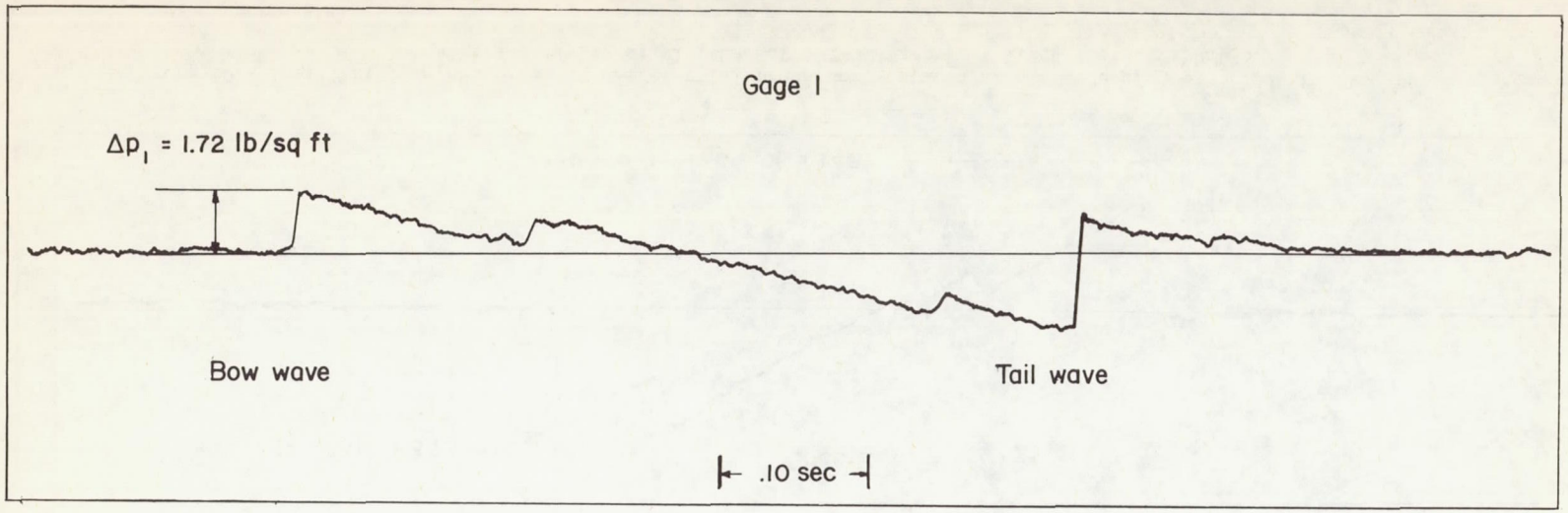

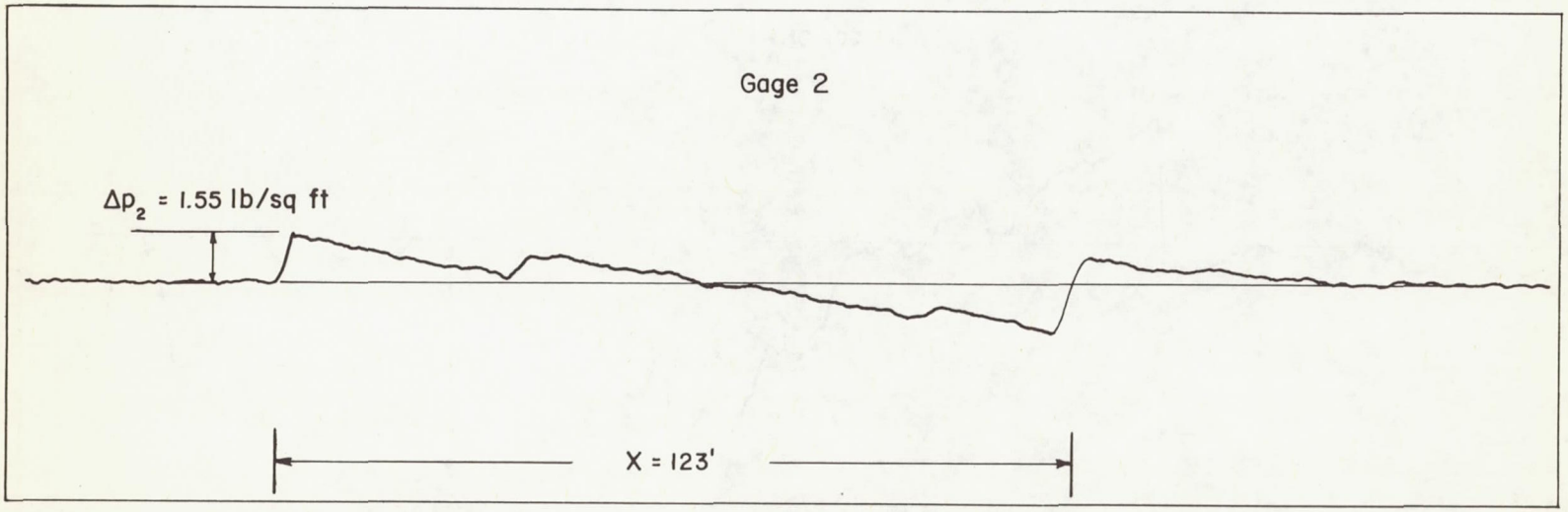

Figure 11.- In-flight time histories of differential pressures measured at altitude of 50,110 feet in flow field of bomber airplane flying at altitude of 48,440 feet (y = 1,820 feet); flight 4.

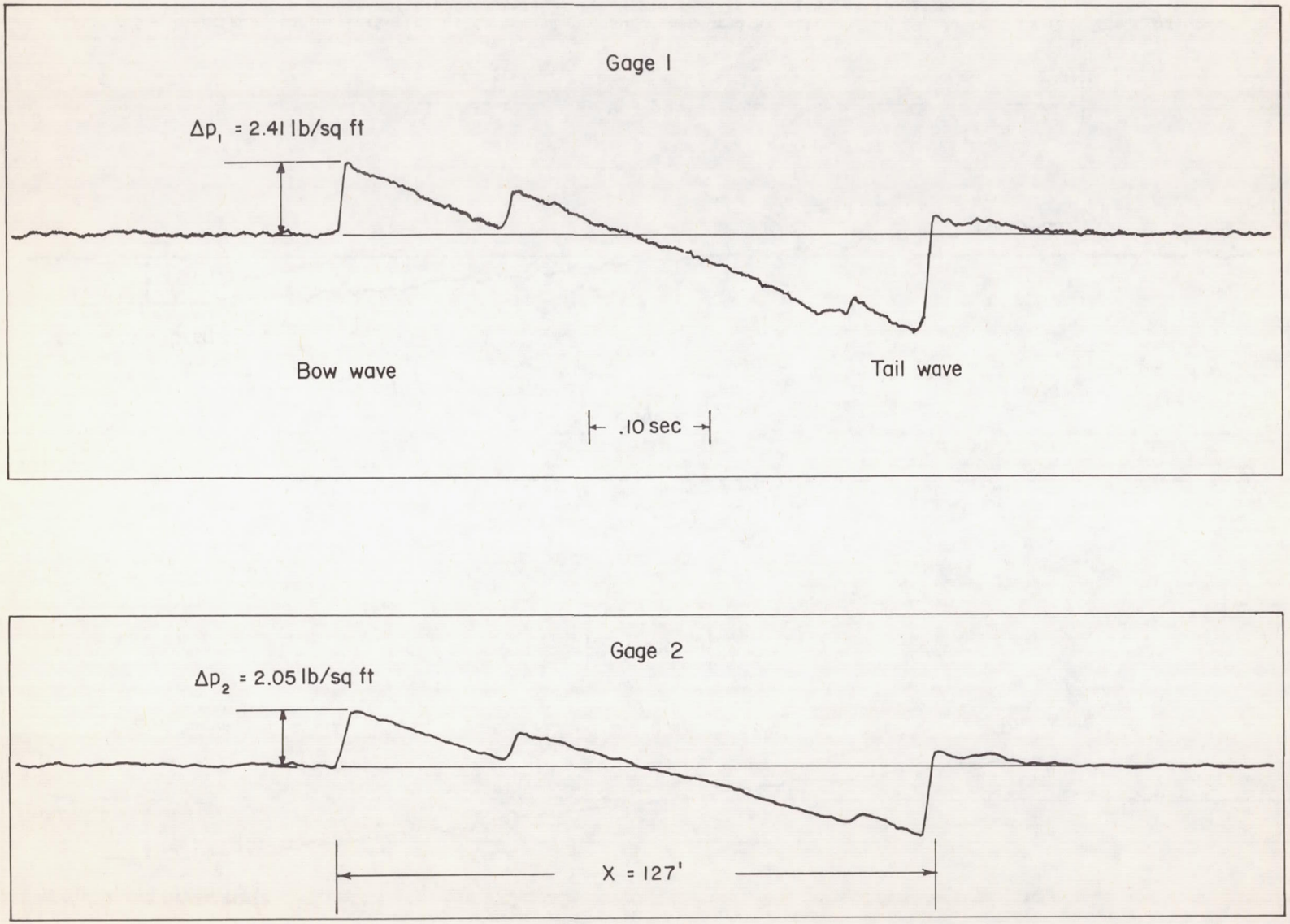

Figure 12.- In-flight time histories of differential pressures measured at altitude of 42,580 feet in flow field of bomber airplane flying at altitude of 40,600 feet (y = 1,994 feet); flight 5.

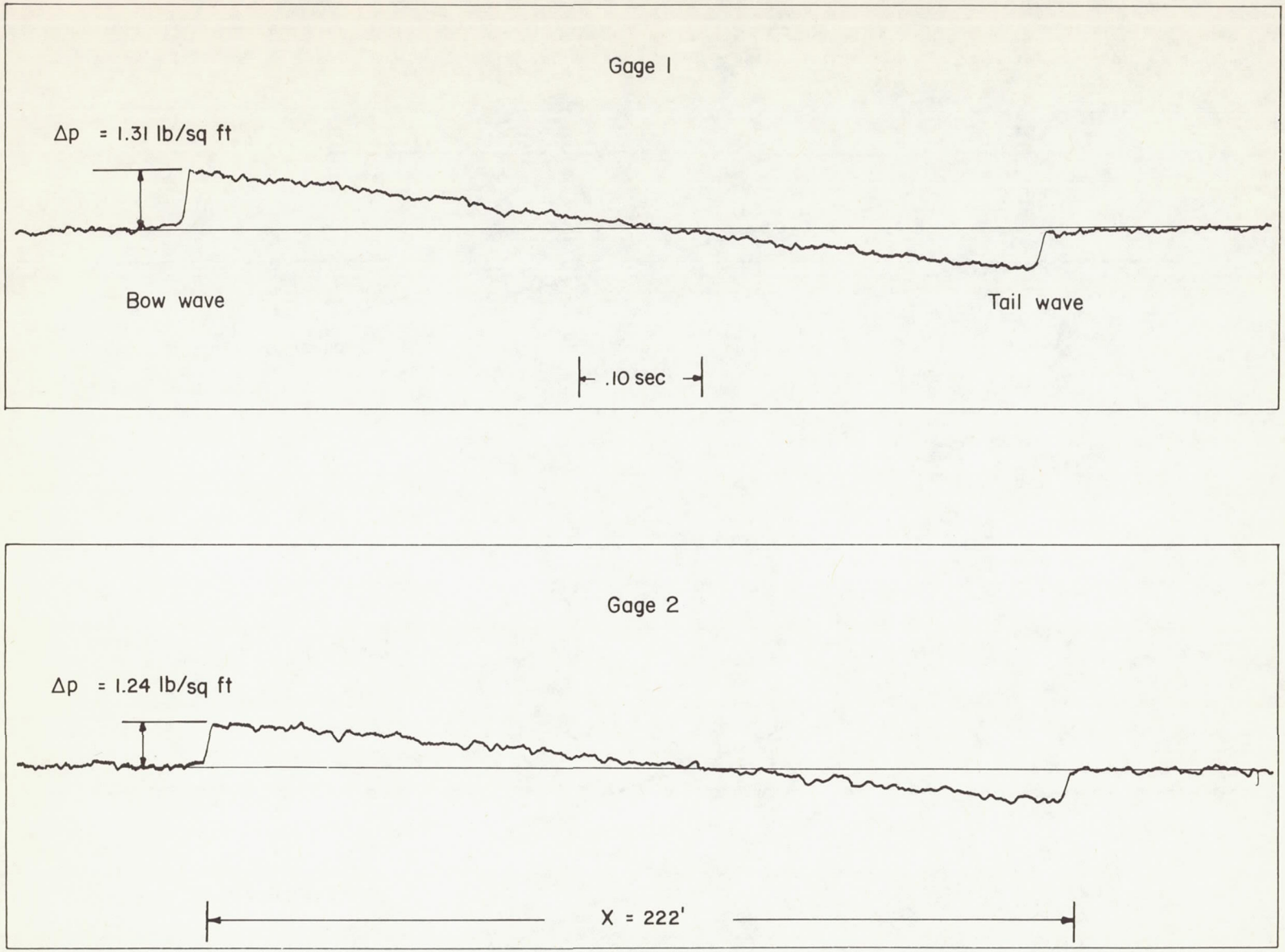

Figure 13.- In-flight time histories of differential pressures measured at altitude of 39,190 feet in flow field of bomber airplane flying at altitude of 48,270 feet (y = 9,155 feet); flight 6.

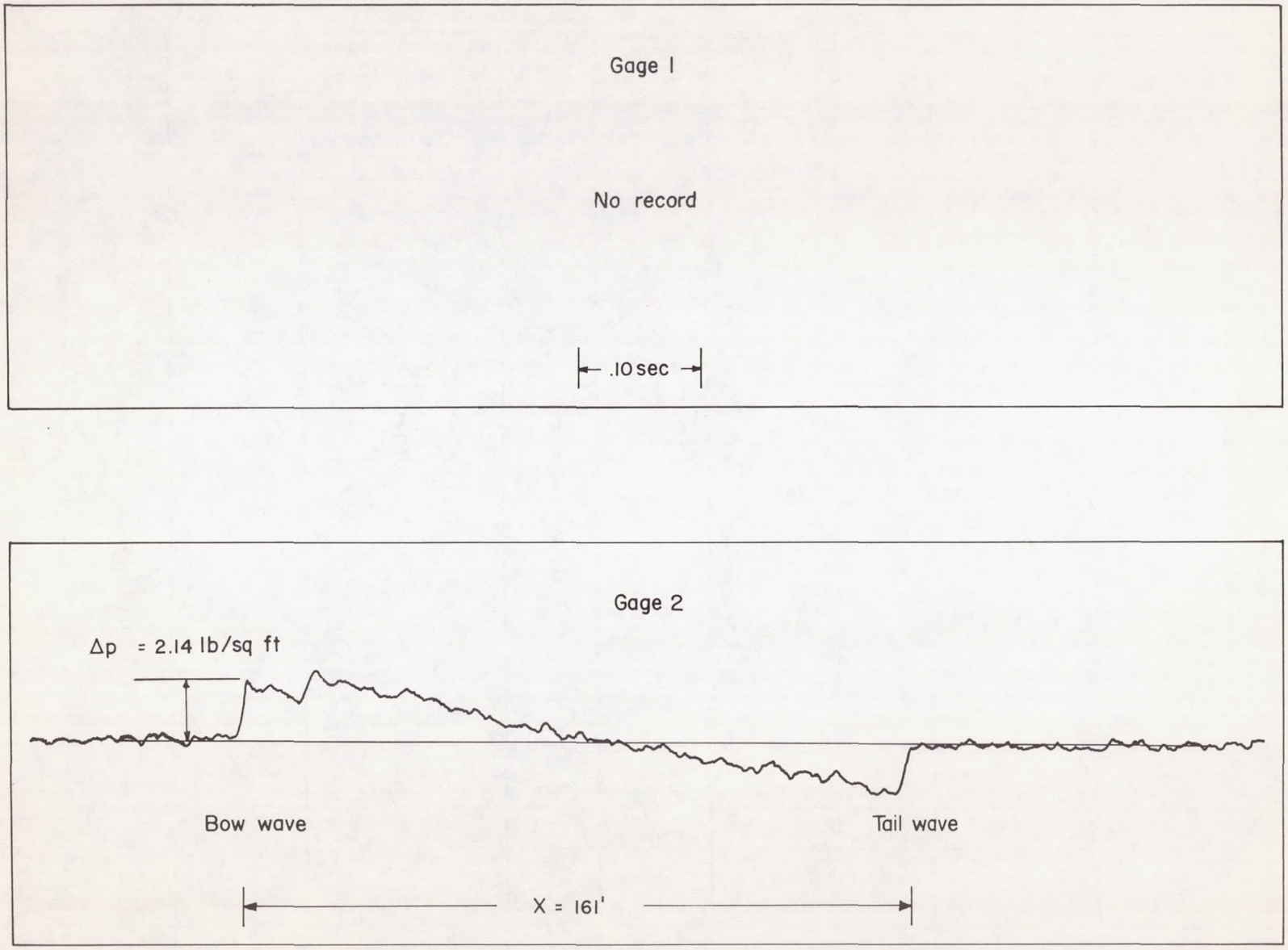

Figure 14.- In-flight time histories of differential pressures measured at altitude of 36,115 feet in flow field of bomber airplane flying at altitude of 40,710 feet (y = 4,615 feet); flight 7.

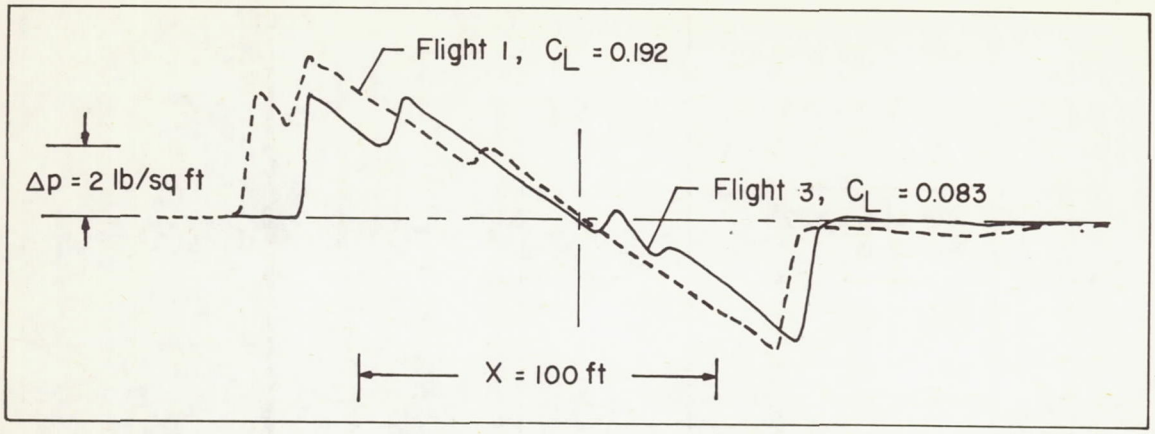

(a) Below airplane.

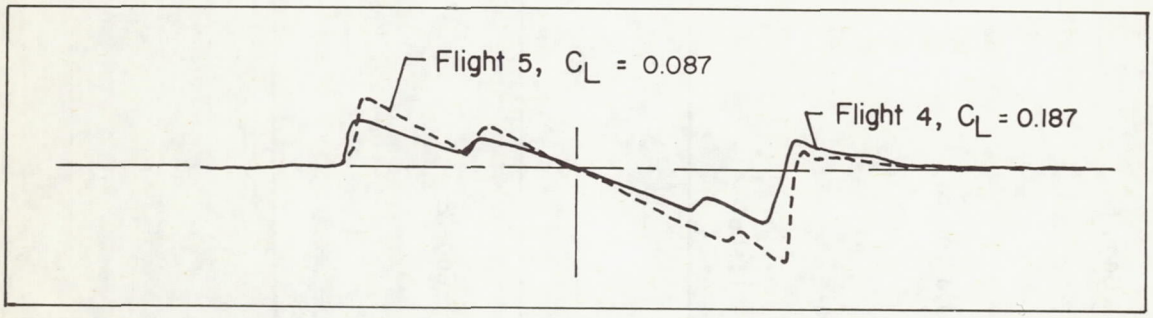

(b) Above airplane.

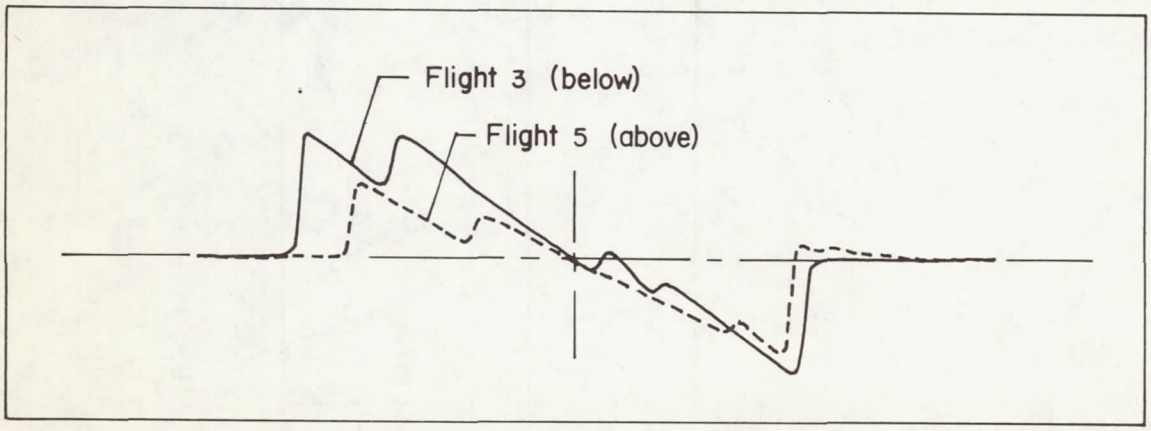

(c) Above and below airplane.

Figure 15.- Effect of lift coefficient and orientation on characteristics of pressure signatures in flow field of bomber airplane. Pressure and distance scales indicated in part (a) are also applicable to (b) and (c).

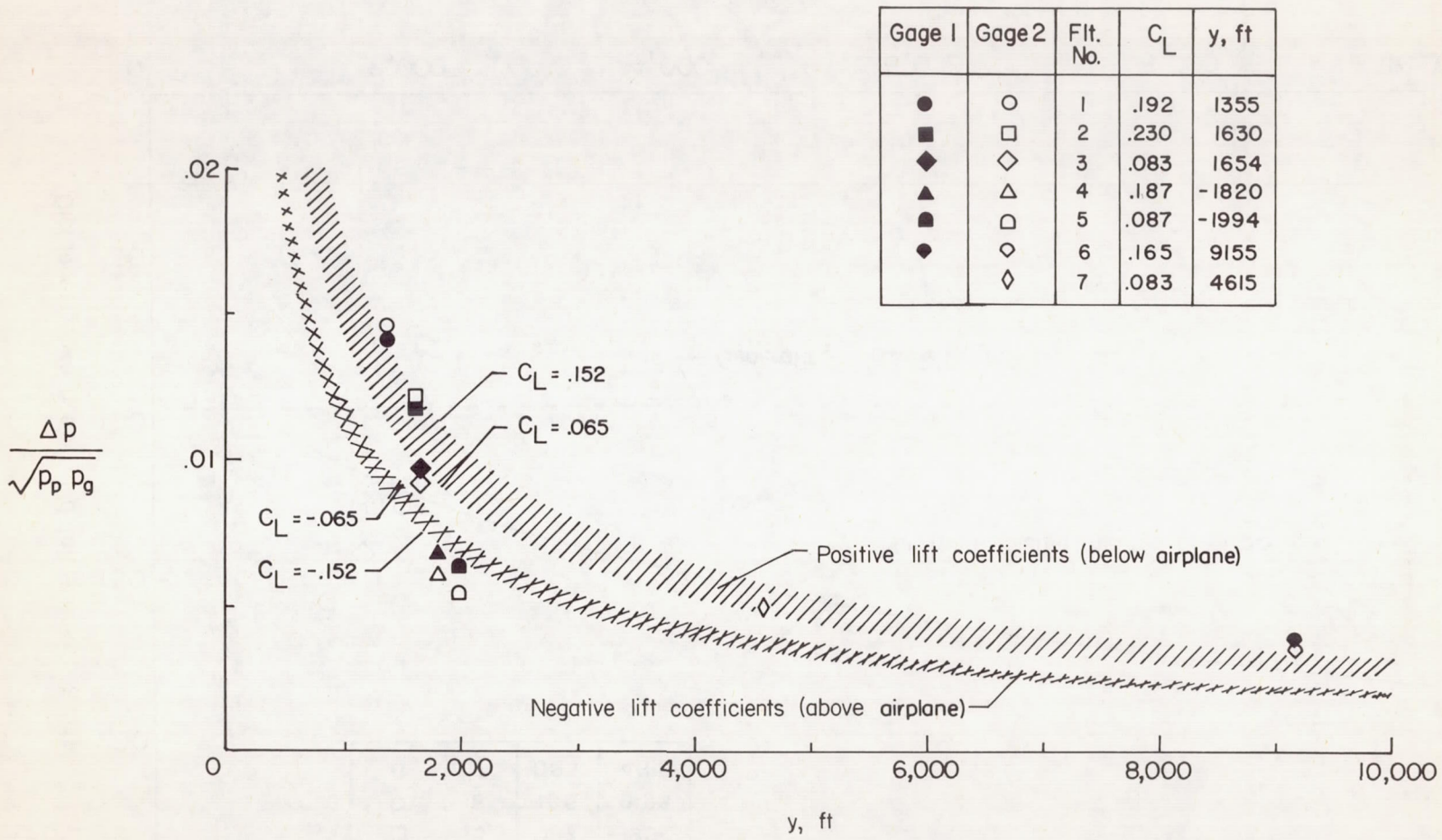

Figure 16.- Comparison of measured and calculated peak shock-wave overpressures as a function of distance above and below the generating airplane. Data are for the generating airplane at altitudes of 40,000 to 49,000 feet and for a range of gross weights.

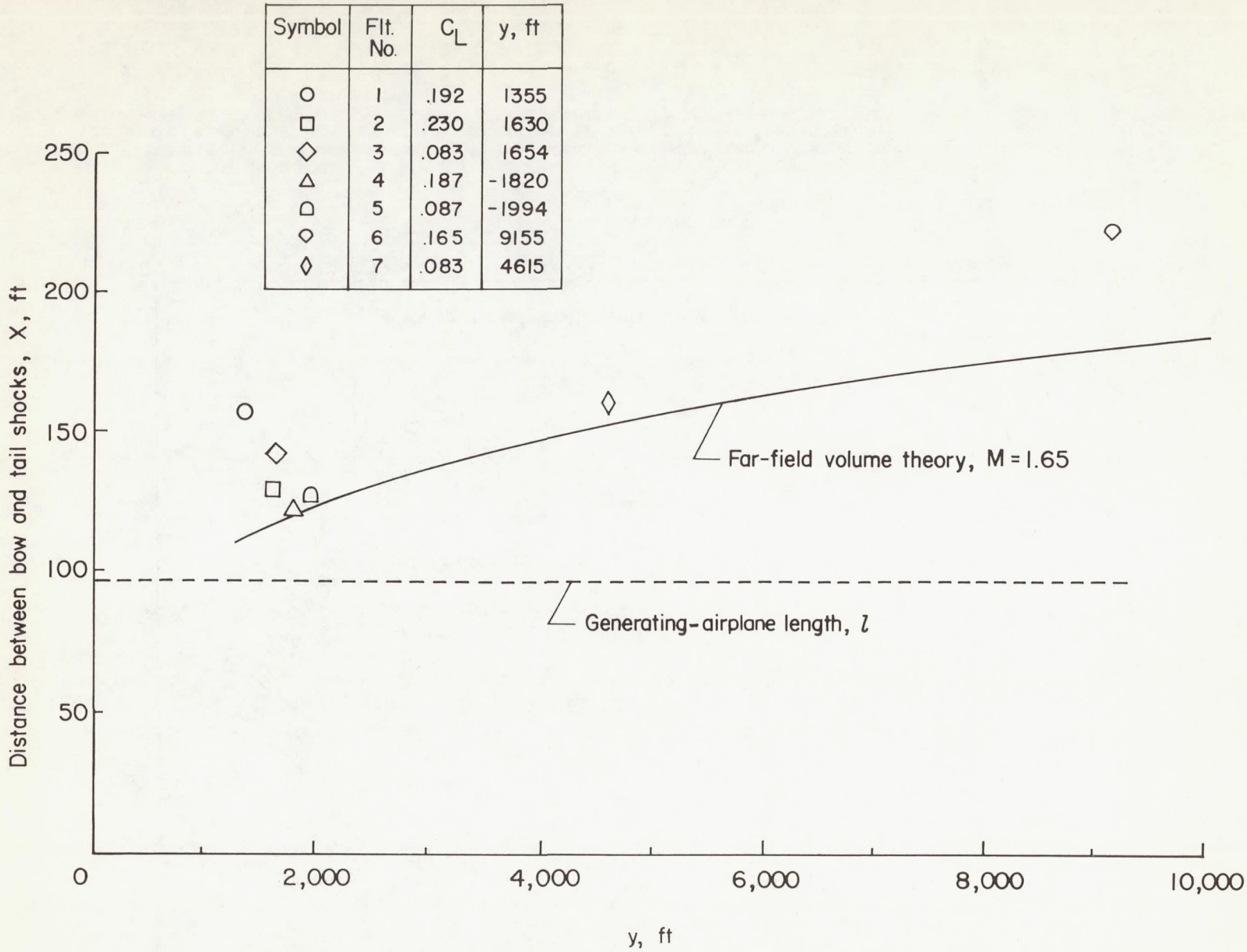

Figure 17.- Comparison of measured and calculated distances between bow wave and tail wave of generating airplane.

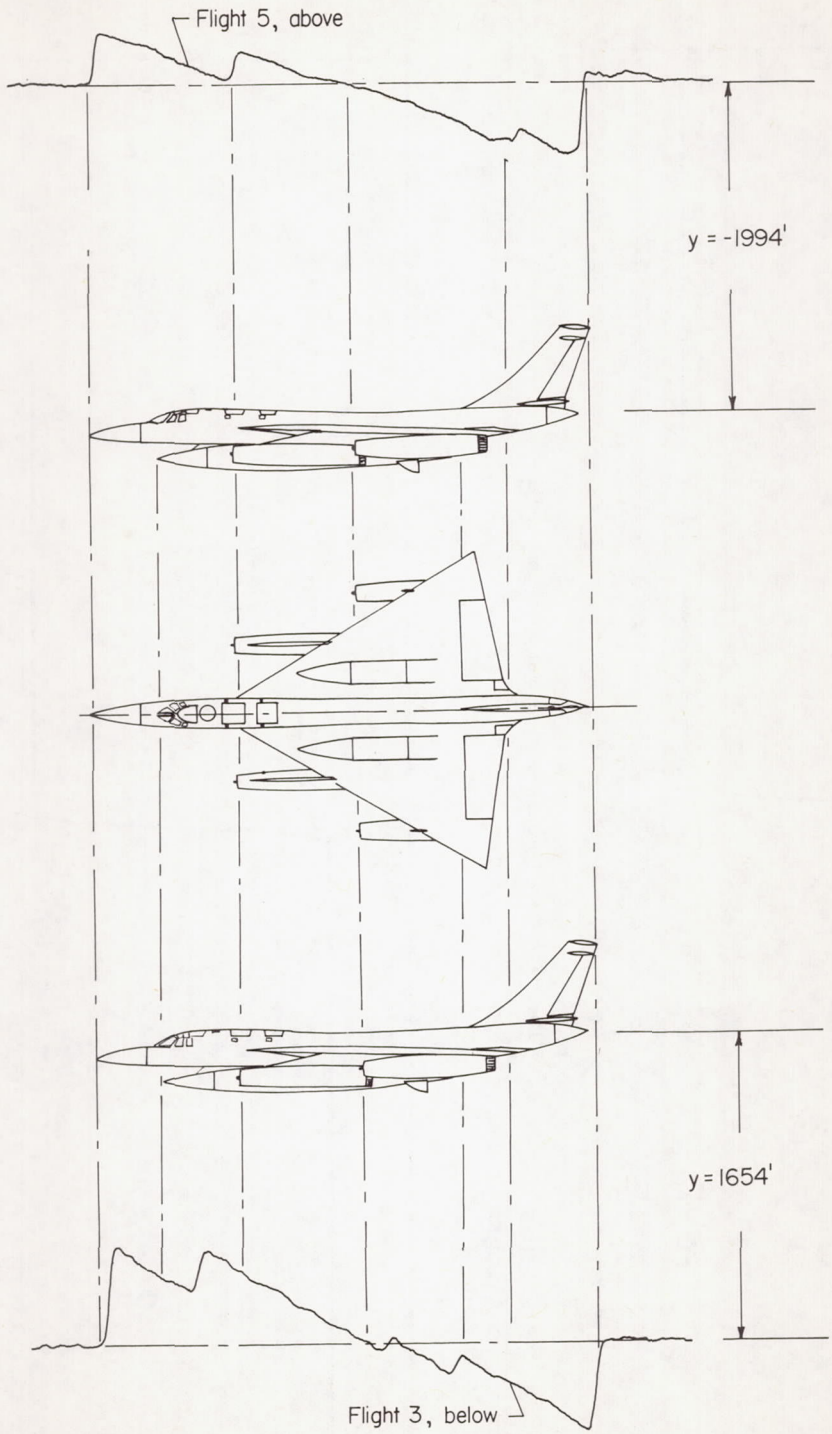

Figure 18.- Planform and side views of bomber airplane with time history of pressure signature as measured above and below airplane. Signature scale has been adjusted to make distance between nose and tail shocks approximately the same as the airplane length.

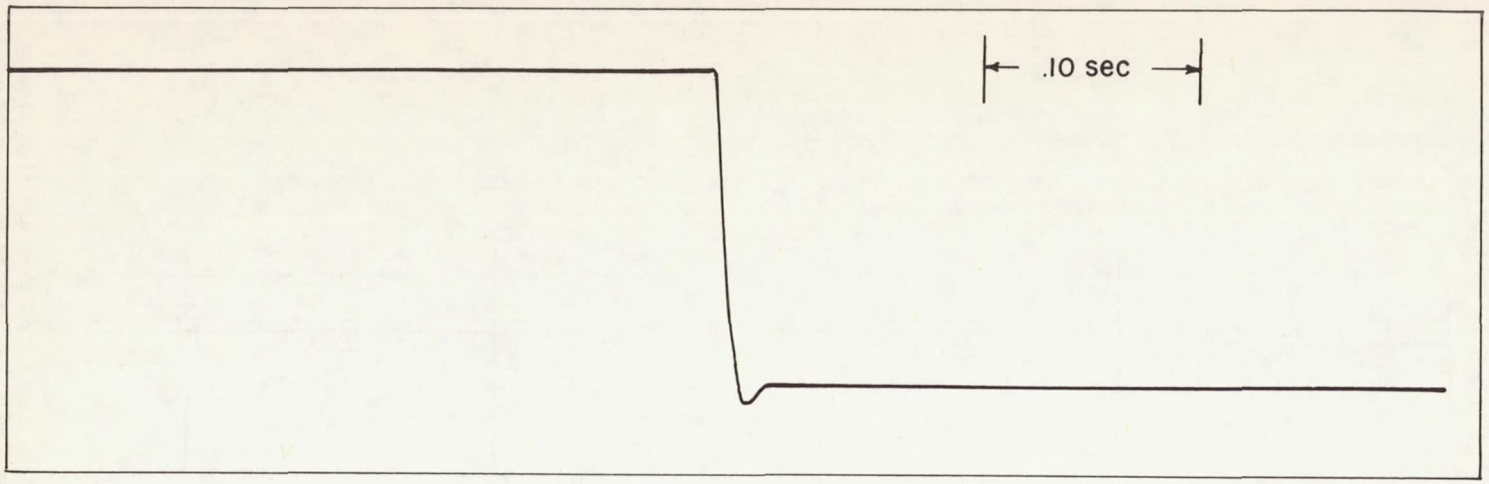

(a) Entire system (pressure gage and galvanometer).

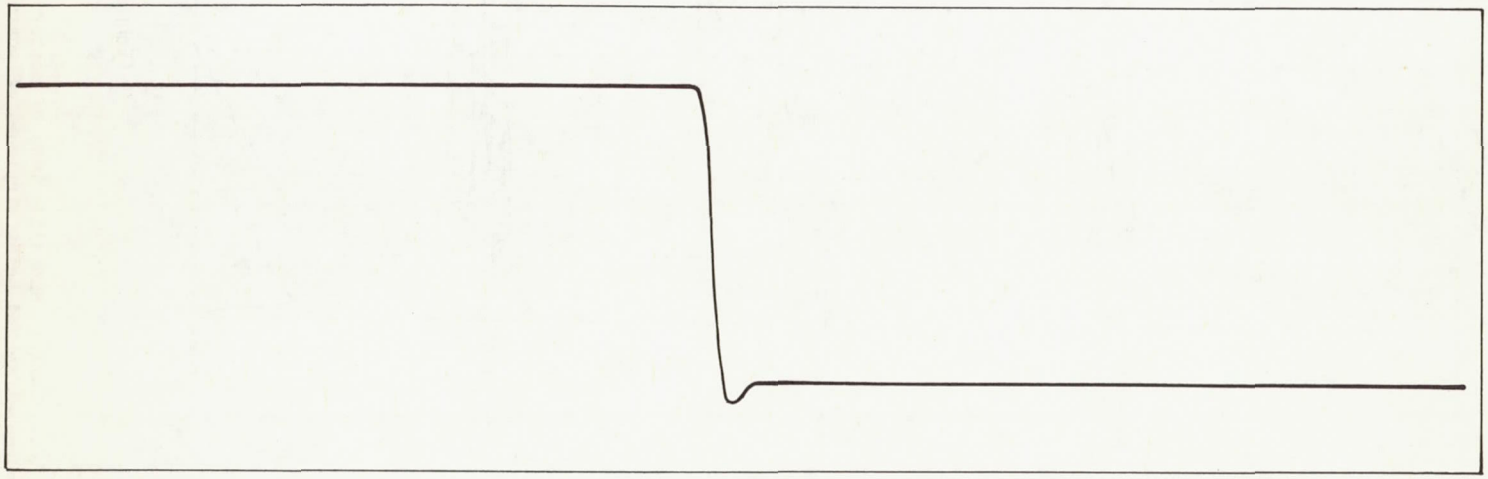

(b) Galvanometer only.

Figure 19.- Response characteristics of pressure instrumentation used for in-flight measurements.

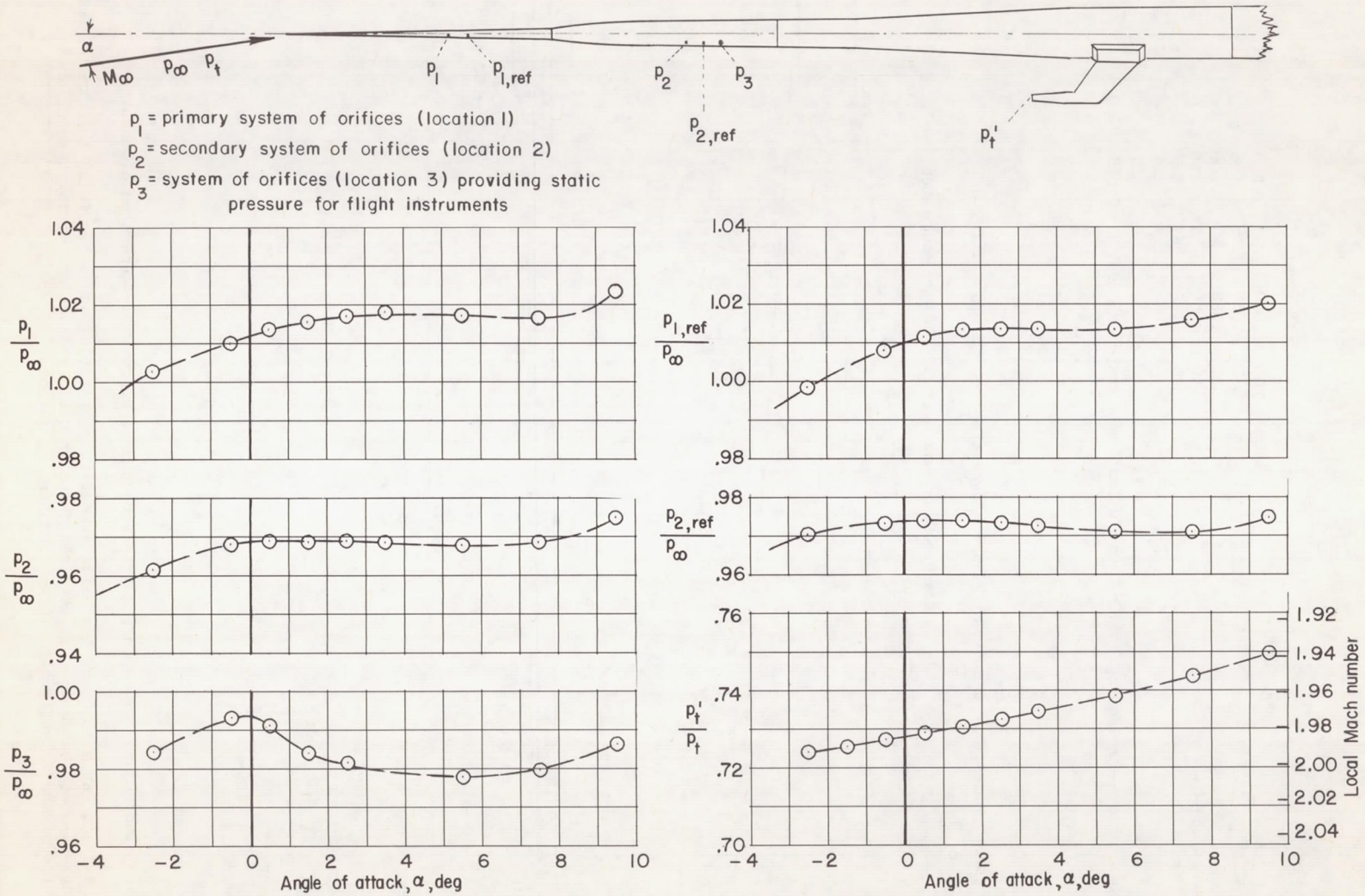

Figure 20.- Steady-state calibration of flight probe at angles of attack from -2.5° to 9.5°, as obtained from tests in the Langley 4-foot supersonic pressure tunnel (pressure orifices at bottom of probe). $M_\infty \approx 2.01$; $p_\infty \approx 185$ lb/sq ft.

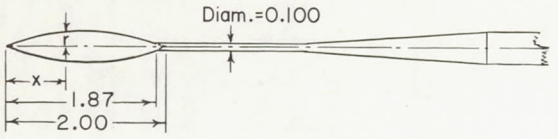

Body ordinates

x	r	x	r
0.00	0.000	1.00	0.200
.10	.038	1.25	.188
.25	.088	1.50	.150
.50	.150	1.75	.088
.75	.188	1.87	.050

(a) Disturbance-generating body of revolution (same shape as model D of ref. 8).

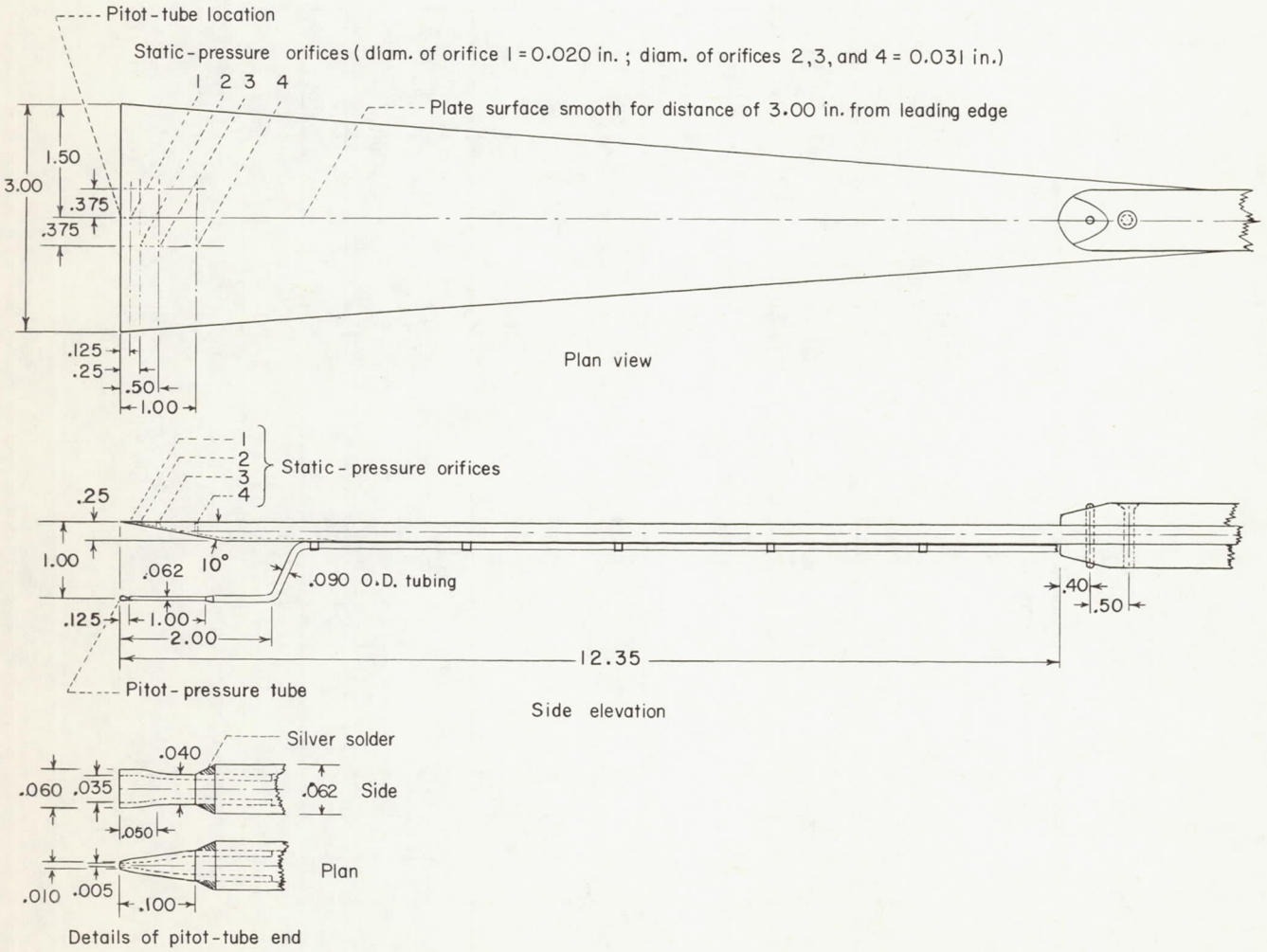

(b) Survey instrument for measuring pressure changes across body-generated disturbance.

Figure 21.- Wind-tunnel apparatus and test arrangement for generating and determining the strength of an axisymmetrical disturbance used in obtaining experimental evidence concerning the reflection characteristics of the flight probe. Dimensions are in inches.

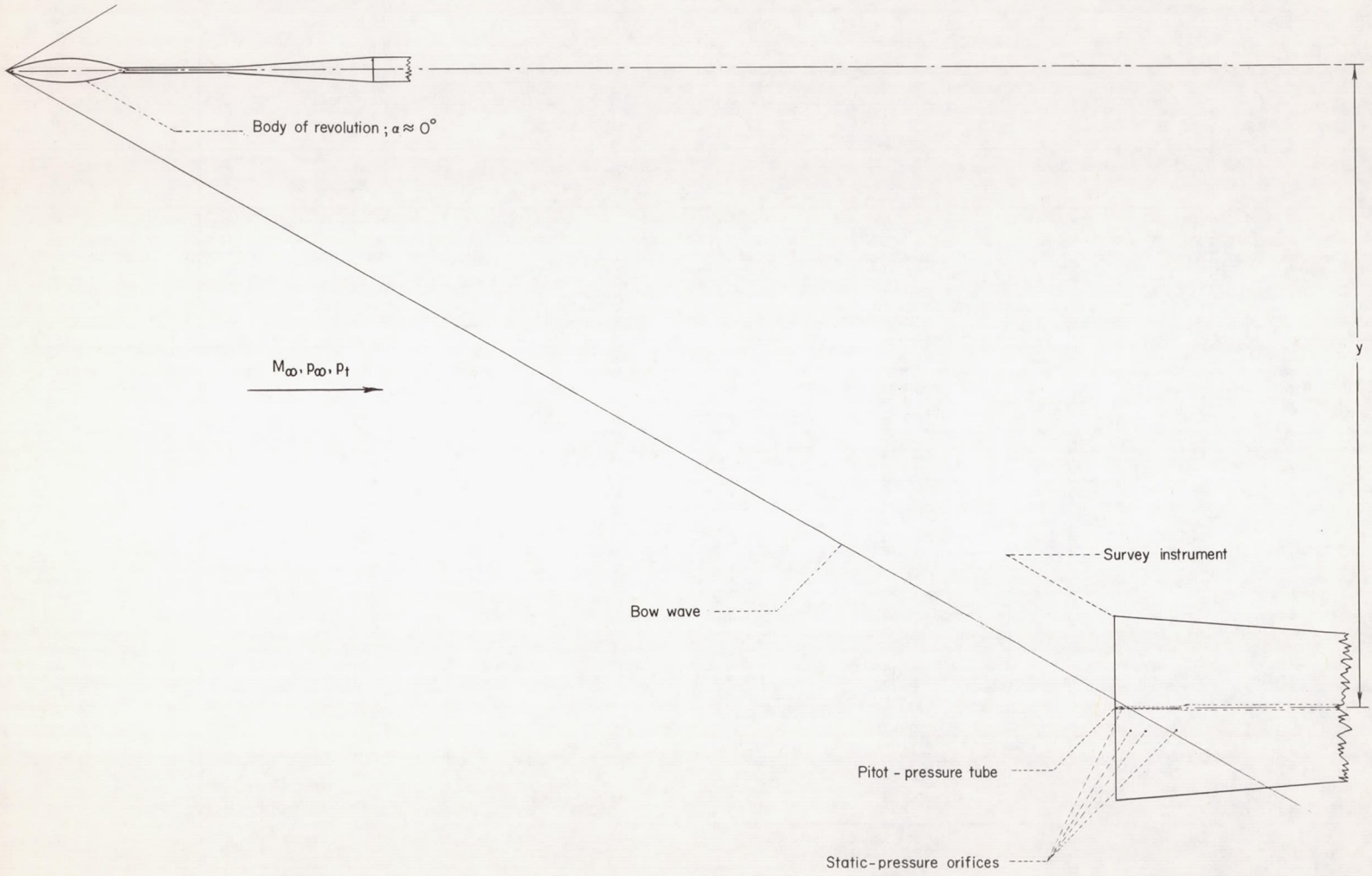

(c) Arrangement for measuring pressure changes across disturbance by use of survey instrument oriented to minimize wave-reflection effects.

Figure 21.- Concluded.

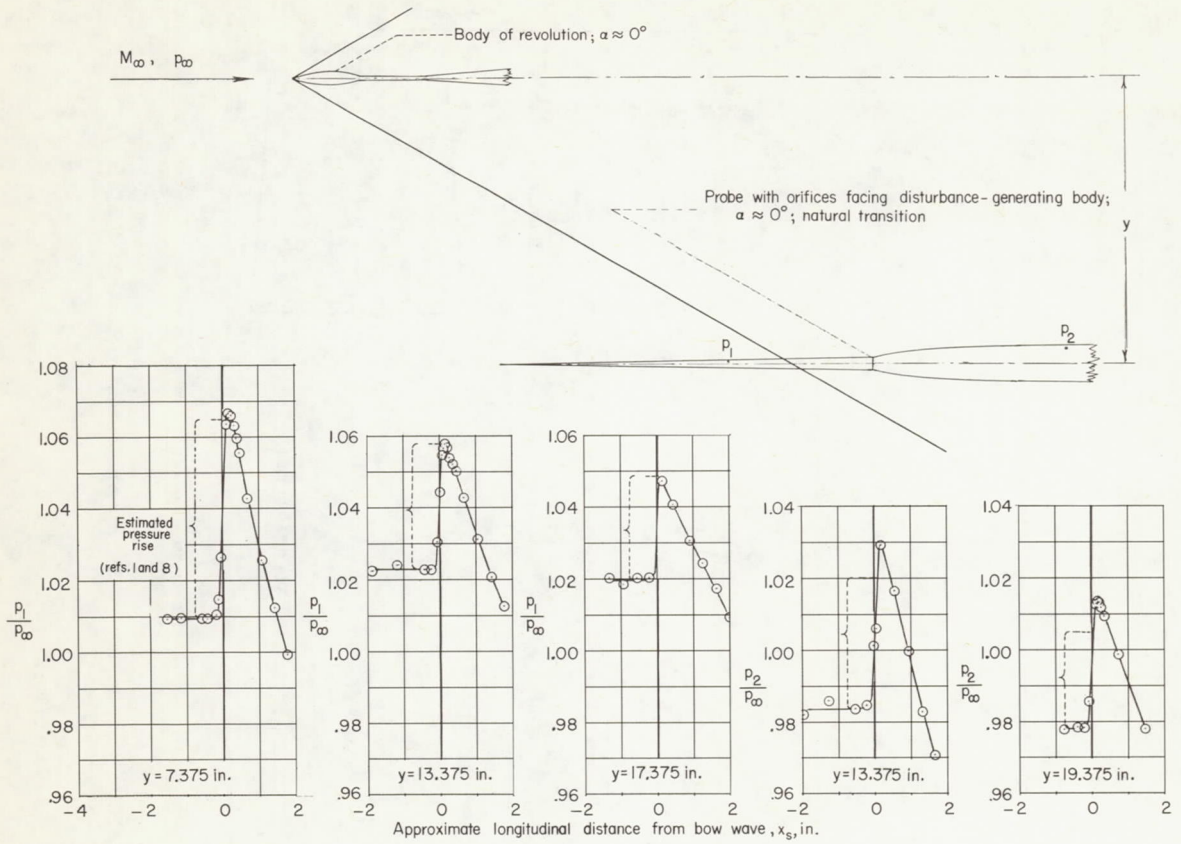

(a) Probe-indicated pressure changes across body-generated bow wave.

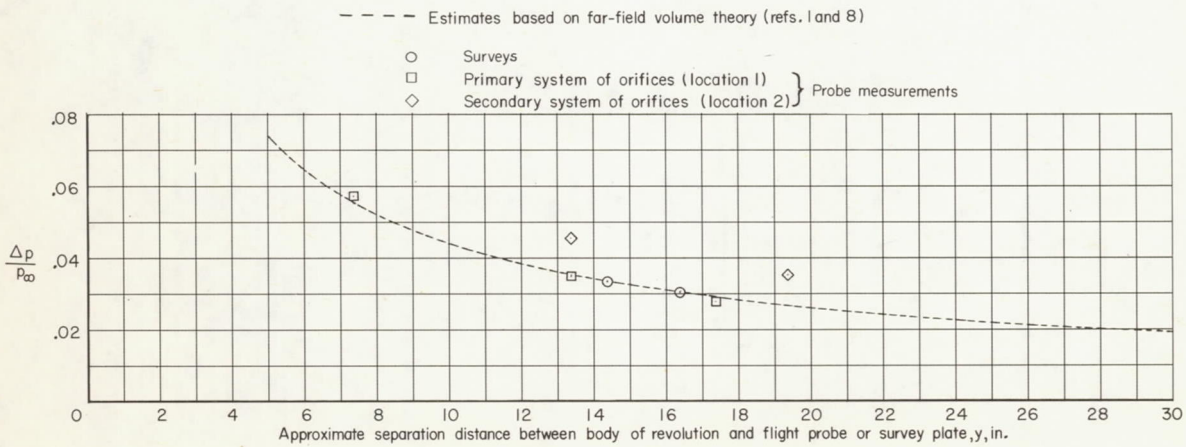

(b) Comparisons of estimated and measured maximum pressure rises across bow wave.

Figure 22.- Flight-probe capability for sensing static-pressure changes across an axisymmetrical disturbance (bow wave generated by body of revolution), as evidenced by comparisons of probe-indicated, survey-indicated, and estimated pressure changes across bow wave. $M_\infty \approx 2.01$.